

24 an NMB of -8.8%. PM_{2.5} concentrations are moderately overpredicted with an NMB of 23.3% at
25 rural sites, but slightly underpredicted with an NMB of -10.8% at urban/suburban sites. In general,
26 the model performs relatively well for chemical and meteorological variables, and not as well for
27 aerosol-cloud-radiation variables. Cloud-aerosol variables including aerosol optical depth, cloud
28 water path, cloud optical thickness, and cloud droplet number concentration are generally
29 underpredicted on average across the continental U.S. Overpredictions of several cloud variables
30 over eastern U.S. result in underpredictions of radiation variables (such as GSW with an MB of -
31 5.7 W m⁻²) and overpredictions of shortwave and longwave cloud forcing (MBs of ~7 to 8 W m⁻²)
32 which are important climate variables. While the current performance is deemed to be acceptable,
33 improvements to the bias-correction method for CESM downscaling and the model
34 parameterizations of cloud dynamics and thermodynamics, as well as aerosol-cloud interactions
35 can potentially improve model performance for long-term climate simulations.

36 **KEYWORDS:** Online-Coupled WRF/Chem; Climate, Air Quality, the Representative
37 Concentration Pathway Scenarios, Climatological Evaluation; Chemistry-Climate Interactions

38 **1. Introduction**

39 Regional atmospheric models have been developed and applied for high resolution climate,
40 meteorology, and air quality modeling in the past few decades. Comparing to global models with
41 a coarser domain resolution (Leung et al., 2003) those regional models have advantages over
42 global models because they can more accurately represent mesoscale variability (Feser et al.,
43 2011), and also better predict the local variability of concentrations of specific species such as
44 black carbon and sulfate (Petikainen et al., 2012). General circulation models (GCMs) and global
45 chemical transport models (GCTMs) are usually downscaled to regional meteorological models
46 such as the Weather Research and Forecasting model (WRF) (Caldwell et al., 2009; Gao et al.,

47 2012), regional climate models such as REMO-HAM (Petikainen et al., 2012), the regional
48 modeling system known as Providing Regional Climates for Impacts Studies (PRECIS) (Jones et
49 al., 2004; Fan et al., 2014), and a number of European models described in Jacob et al. (2007), as
50 well as regional CTMs such as the Community Multiscale Air Quality Model (CMAQ) (Penrod et
51 al., 2014; Xing et al., 2015). These regional models are used for climate/meteorology or air quality
52 simulations. Some are applied for more than ten years (Caldwell et al., 2009; Warrach-Sagi et al.,
53 2013; Xing et al., 2015). However these regional models either lack the detailed treatment of
54 chemistry (e.g., in WRF), or use prescribed chemical concentrations (e.g., REMO-HAM uses
55 monthly mean oxidant fields for several chemical species), or do not have online-coupled
56 meteorology and chemistry (e.g., in CMAQ). In addition, the past regional model simulations and
57 analyses have mainly focused on meteorological parameters such as surface temperature and
58 precipitation, cloud variables such as net radiative cloud forcing, and chemical constituents such
59 as ozone. Regional climate model simulations tend to focus on significant climatic events such as
60 extreme temperatures (very cold or very hot) (Dasari et al., 2014), heat waves, heavy precipitation,
61 drought, and storms (Beniston et al., 2007), rather than the important air quality and climate
62 interactions. In addition, the impacts of complex chemistry-aerosol-cloud-radiation-climate
63 feedbacks on future climate change remain uncertain, and these feedbacks are most accurately
64 represented using online-coupled meteorology and chemistry models (Zhang, 2010; IPCC, 2013).
65 An online-coupled meteorology and chemistry model, however, is more computationally
66 expensive compared to an offline-coupled model (Grell et al., 2004), and thus requires significant
67 computing resources for their long-term (a decade or longer) applications. With rapid increases in
68 the availability of high performance computing resources on the petaflop scale, however, long
69 term simulations using online-coupled models have become possible in recent years. For example,

70 recently, the WRF model has been coupled online to the CMAQ model with the inclusion of
71 aerosol indirect effects to study chemistry and climate interactions (Yu et al., 2014).

72 The online-coupled WRF model with Chemistry (WRF/Chem) has been updated with a
73 suite of physical parameterizations from the Community Atmosphere Model version 5 (CAM5)
74 (Neale et al., 2010) so that the physics in the global CAM5 model is consistent with the regional
75 model for downscaling purposes (Ma et al., 2014). There are also limited applications of dynamical
76 downscaling (Gao et al., 2013) under the new Intergovernmental Panel on Climate Change (IPCC)
77 Fifth Assessment Report's Representative Concentration Pathway (RCP) scenarios (van Vuuren
78 et al., 2011). Gao et al. (2013) applied dynamic downscaling to link the global-climate-chemistry
79 model CAM-Chem with WRF and CMAQ using RCP 8.5 and RCP 4.5 emissions to study the
80 impacts of climate change and emissions on ozone (O₃). Molders et al. (2014) downscaled the
81 Community Earth System Model (CESM) (Hurrell et al., 2013) to drive the online-coupled
82 WRF/Chem model over Southeast Alaska using RCP 4.5 emissions; however, their study did not
83 address the feedback processes between chemistry and meteorology. This study evaluates the
84 online-coupled regional WRF/Chem model, which takes into account gas and aerosol-phase
85 chemistry, as well as aerosol direct and indirect effects. WRF/Chem is used to simulate the
86 "current" climate scenario for 10 years, from 2001 to 2010 using the RCP 8.5 emissions and
87 boundary conditions from an updated version of CESM with advanced chemistry and aerosol
88 treatments over continental U.S. (CONUS) (He et al., 2015; Glotfelty et al., 2015) with a focus on
89 air-quality and climate interactions. Both CESM and WRF/Chem include similar gas-phase
90 chemistry and aerosol treatments. To our best knowledge, this study is the first to report the
91 WRF/Chem simulation, evaluation, and analyses over a period of 10 years (i.e., 2001-2010) to
92 assess if the model is able to accurately simulate decadal long air quality and climatology by taking

93 into account feedback processes between chemistry and meteorology. This study also assesses
94 whether the RCP8.5 emissions for the 10-year period are robust enough to produce satisfactory
95 performance against observations with WRF/Chem.

96 **2. Model Set-up and Evaluation Protocol**

97 **2.1 Model Configurations and Simulation Design**

98 The model used is the modified WRF/Chem v3.6.1 with updates similar to those
99 implemented into WRF/Chem v3.4.1 as documented in Wang et al. (2014). The main updates
100 include the implementation of an extended version of Carbon Bond 2005 (CB05) (Yarwood et al.,
101 2005) gas-phase mechanism with the chlorine chemistry (Sarwar et al., 2007) and its coupling with
102 the Modal for Aerosol Dynamics in Europe/Volatility Basis Set (MADE/VBS) (Ahmadov et al.,
103 2012). MADE/VBS incorporates a modal aerosol size distribution, and includes an advanced
104 secondary organic aerosol (SOA) treatment based on gas-particle partitioning and gas-phase
105 oxidation in volatility bins. The CB05-MADE/VBS option has also been coupled to existing model
106 treatments of various feedback processes such as the aerosol semi-direct effect on photolysis rates
107 of major gases, and the aerosol indirect effect on cloud droplet number concentration (CDNC) and
108 resulting impacts on shortwave radiation. The main physics and chemistry options used in this
109 study as well as their corresponding references can be found in Table 1. The simulations are
110 performed at a horizontal resolution of 36-km with 148×112 horizontal grid cells over the
111 CONUS domain and parts of Canada and Mexico, and a vertical resolution of 34 layers from the
112 surface to 100-hPa. Considering the decadal applications of WRF/Chem in this work which is
113 much longer than many past WRF/Chem applications, the simulations are reinitialized monthly
114 (rather than 1-4 days used in most past WRF/Chem applications to short-term episodes that are on
115 an order of months up to 1-year, e.g., Zhang et al., 2012a, b; Yahya et al., 2014, 2015b) to constrain

116 meteorological fields toward National Centers for Environmental Prediction (NCEP) reanalysis
117 data while allowing chemistry-meteorology feedbacks within the system. As discussed in Sections
118 3.1 and 3.3, the reinitialization frequency of 1-month may be too large to constrain some of the
119 meteorological fields such as moistures, which in turn affect other parameters, and a more frequent
120 reinitialization may be needed to improve the model performance. The impact of the frequency of
121 the reinitialization on simulated meteorological and cloud parameters will be further discussed in
122 Sections 3.1 and 3.2. A list of acronyms used in this paper can be found in Table S1.

123 **2.2 Processing of Emissions and Initial Conditions (ICs)/Boundary Conditions (BCs)**

124 Global RCP emissions are available as monthly-average emissions for 2000, 2005, and for
125 every 10 years between 2010 and 2100, at a grid resolution of $0.5^{\circ} \times 0.5^{\circ}$ (Moss et al., 2010; van
126 Vuuren et al., 2011). The RCP emissions in 2000, 2005, and 2010 are used to cover the 10-year
127 emissions needed for WRF/Chem simulations, i.e., the periods of 2001 – 2003, 2004 – 2006, and
128 2007 – 2010, respectively. Processing global RCP emissions in 2000, 2005, and 2010 into regional,
129 hourly emissions needed for the 10-year WRF/Chem simulations requires essentially three main
130 tasks. These include 1) mapping the RCP species to CB05 speciation used in WRF/Chem; 2) re-
131 gridding the RCP emissions from $0.5 \times 0.5^{\circ}$ grid resolution to the 36×36 km grid resolution used
132 for regional simulation over North America; and 3) applying species and location dependent
133 temporal allocations (i.e., emissions variation over time) to the re-gridded RCP emissions. Table
134 S2 shows the species mapping between RCP species and CB05 species. To map the RCP species
135 to CB05 speciation, some assumptions are made due the relatively detailed speciation required by
136 CB05. Some of the CB05 species are directly available in RCP; however, others are lumped into
137 RCP groups, for example, the “other alkanals” and “hexanes and higher alkanes” in the RCP
138 groups can be considered to approximately represent the acetaldehyde and higher aldehydes

139 emissions required by CB05, respectively (Table S2). For the CB05 species such as ethanol,
140 methanol, internal and terminal olefin carbon bonds in the gas-phase, and elemental and organic
141 carbon in the accumulation mode of the aerosol particles, other RCP groups are used to
142 approximate these emissions (Table S2). For the remaining CB05 species that are not available in
143 RCP (i.e. chlorine, HCl, HONO, NH_4^+ , NO_3^- , PAR, unspciated $\text{PM}_{2.5}$, H_2SO_4 , and SO_4^{2-}), their
144 2000 emissions are based on the 2002 National Emission Inventory (NEI) (version 3,
145 <http://www.epa.gov/ttn/chief/emch/>), while their 2005 and 2010 emissions are based on the 2008
146 NEI-derived emissions (version 2) from the Air Quality Modelling Evaluation International
147 Initiative (AQMEII) project as described in Pouliot et al. (2015), which include year-specific
148 updates for on/off road transport, wildfires and prescribed fires, and Continuous Emission
149 Monitoring-equipped point sources. To re-grid the RCP emissions, the RCP rectilinear grid is first
150 interpolated to a WRF/Chem curvilinear grid using a simple inverse distance weighting (NCAR
151 Command Language Function – `rgrid2rcm`), and a subset of the RCP grid that covers the
152 WRF/Chem CONUS domain is then extracted. To derive a temporal allocation for monthly-
153 averaged RCP emissions, hourly emission profiles are taken from those used in-house WRF/Chem
154 simulations over CONUS during 2001 (Yahya et al., 2015a), and 2006 and 2010 as part of the
155 AQMEII project (Yahya et al., 2014, 2015b). The emissions for those existing in-house
156 simulations were generated based on the 2002 NEI, the emissions were generated with the Sparse
157 Matrix Operator Kernel Emissions (SMOKE) model version 2.3. The emissions for the existing
158 in-house 2006 and 2010 simulations were generated based on the pre-merged emissions provided
159 by the U.S. EPA, which were derived from the 2008 NEI with year-specific section emissions for
160 2006 and 2010 as part of the AQMEII. SMOKE version 3.4 was used to prepare the spatially,
161 temporally, and chemically speciated “model-ready” emissions for the existing in-house 2006 and

162 2010 WRF/Chem simulations. Since NEI is updated and released every three years, the temporal
 163 profiles of emissions used in SMOKE for 2002, 2006 and 2010 are assumed to be valid for 3-4
 164 years around the NEI years, i.e., 2001-2003, 2004-2006, and 2007-2010, respectively. The
 165 temporal allocations applied to the RCP emissions are therefore based on the SMOKE model's
 166 profiles for each species and source location, and include non-steady-state emissions rates (i.e.,
 167 seasonal, weekday or weekend, and diurnal variability) that are valid for the entire simulation
 168 periods of 2001-2010. Specifically, the hourly re-gridded RCP emission rates for each species E ,
 169 or E_{hr}^{RCP} are calculated by

$$170 \quad E_{hr}^{RCP}(t, z, lat, lon) = E_{mon}^{RCP}(z, lat, lon) * \left[\frac{E_{hr}^{WRF}(t, z, lat, lon)}{E_{mon}^{WRF}(z, lat, lon)} \right] \quad (1)$$

171 where E_{mon}^{RCP} , E_{mon}^{WRF} , and E_{hr}^{WRF} represent the original monthly-averaged RCP emissions rates, the
 172 monthly-averaged WRF/Chem emissions rates, and the hourly WRF/Chem emission rates,
 173 respectively, which are valid at each model time t , layer z , and lat and lon grid points. The RCP
 174 elevated source emissions for sulfur dioxide (SO₂), sulfate (SO₄²⁻), elemental carbon (EC) and
 175 organic carbon (OC) were also incorporated into the model-ready emissions for WRF/Chem using
 176 steps 1) – 3) and Eq. (1) above. Lastly, RCP aircraft source emissions for EC, nitric oxide (NO),
 177 and nitrogen dioxide (NO₂) are directly injected into the closest model layers. No temporal
 178 allocations are applied to the RCP aircraft source emissions.

179 Biogenic emissions are calculated online using the Model of Emissions of Gases and
 180 Aerosols from Nature version 2 (MEGAN2) (Guenther et al., 2006). Emissions from dust are based
 181 on the online Atmospheric and Environmental Research Inc. and Air Force Weather Agency
 182 (AER/AFWA) scheme (Jones and Creighton, 2011). Emissions from sea salt are generated based
 183 on the scheme of Gong et al. (1997).

184 The chemical and meteorological ICs/BCs come from the modified CESM/CAM5 version
185 1.2.2 with updates by He et al. (2014) and Glotfelty et al. (2015) developed at the North Carolina
186 State University (CESM_NCSU). WRF/Chem and CESM both use the CB05 gas-phase
187 mechanism (Yarwood et al., 2005), however, WRF/Chem includes additional chlorine chemistry
188 from Sarwar et al. (2007), whereas CESM_NCSU uses a modified version of CB05, the CB05
189 Global Extension (CB05GE) by Karamchandani et al. (2012). In addition to original reactions in
190 CB05 and chlorine chemistry of Sarwar et al. (2007), CB05GE includes chemistry on the lower
191 stratosphere, reactions involving mercury species, and additional heterogeneous reactions on
192 aerosol particles, cloud droplets and on polar stratospheric clouds (PSCs). Both WRF/Chem and
193 CESM_NCSU use a modal aerosol size representation, rather than a sectional size representation.
194 While WRF/Chem includes MADE/VBS with 3 prognostic modes (Ahmadov et al.,
195 2012),CESM_NCSU includes the Modal Aerosol Model with 7 prognostic modes (Liu et al., 2012)
196 is used in CESM_NCSU. In addition to similar gas-phase chemistry and aerosol treatments,
197 CESM_NCSU and WRF/Chem use the same shortwave and longwave radiation schemes (i.e., the
198 Rapid and accurate Radiative Transfer Model for GCM (RRTMG)), though they use different
199 cloud microphysics parameterizations, PBL, and convection schemes. As GCMs generally contain
200 systematic biases which can influence the downscaled simulation, the meteorological ICs/BCs
201 predicted by CESM_NCSU are bias corrected before they are used by WRF/Chem using the
202 simple bias correction technique based on Xu and Yang (2012). Temperature, water vapor,
203 geopotential height, wind, and soil moisture variables available every 6 hours from the NCEP Final
204 Reanalyses (NCEP FNL) dataset are used to correct the ICs and BCs derived based on results from
205 CESM_NCSU for WRF/Chem simulations. In this bias-correction approach, monthly
206 climatological averages for ICs and BCs are first derived from both NCEP and CESM_NCSU

207 cases. The differences between the ICs and BCs from the NCEP and CESM_NCSU climatological
 208 averages are then added onto the CESM_NCSU ICs and BCs to generate bias-corrected
 209 CESM_NCSU ICs/BCs. Assuming that the causes for the biases remain the same in future, this
 210 bias correction technique can also be applied to future year simulations for which NCEP FNL data
 211 is not available.

212 **2.3 Model Evaluation Protocol**

213 The focus of the model evaluation is mainly to assess whether the model is able to
 214 adequately reproduce the spatial and temporal distributions of key meteorological and chemical
 215 variables as compared to observations on a climatological time scale. A scientific question to be
 216 addressed in this work is, is WRF/Chem sufficiently good for regional climate and air quality
 217 simulations on a decadal scale? A climatological month refers to the average of the month for all
 218 the 10 years. For example, January refers to the average for all the months of January from 2001
 219 to 2010. Statistical evaluations such as mean bias (MB), Pearson’s correlation coefficient (R),
 220 normalized mean bias (NMB), normalized mean error (NME) (The definition of those measures
 221 can be found in Yu et al. (2006) and Zhang et al. (2006)) and Index of Agreement (IOA) ranging
 222 from 0 to 1 (Willmott et al., 1981) for major chemical and meteorological variables are included.
 223 IOA can be calculated as,

$$224 \quad IOA = 1 - \frac{\sum_i^N (O_i - S_i)^2}{\sum_i^N (|O_i - \bar{O}| + |S_i - \bar{S}|)^2} \quad (2)$$

225 where O_i and S_i denote time-dependent observations and predictions at time and location i ,
 226 respectively, N is the number of samples (by time and/or location), \bar{O} denotes mean observation
 227 and \bar{S} denotes mean predictions over all time and locations, they can be calculated as:

228
$$\bar{O} = (1/N) \sum_{i=1}^N O_i, \bar{S} = (1/N) \sum_{i=1}^N S_i,$$

229 IOA values range from 0-1, with a value of 1 indicating a perfect agreement.

230 For surface networks with hourly data, e.g., National Climatic Data Center (NCDC), the
231 observational data are paired up with the simulated data on an hourly basis for each site. The
232 observational data and simulated data are averaged out for each site. The statistics are then
233 calculated based on the site-specific data pairs. The satellite-derived data are usually available on
234 a monthly basis, and the simulated data are also averaged out on a monthly basis. The satellite-
235 derived data are regridded to the same domain and number of grid cells similar to the simulated
236 data. The time dimension is removed for the climatological evaluation, the statistics are based on
237 a site-specific average or a grid cell average. The statistics are then calculated based on the paired
238 satellite-derived vs. simulated grid cell values. The spatial and temporal analyses include spatial
239 plots of MB over CONUS, spatial overlay plots of averaged simulated and observational data,
240 monthly climatologically-averaged time series of major meteorological and chemical variables,
241 annual average time series; probability distribution functions of major meteorological and
242 chemical variables, and spatial plots of major aerosol and cloud variables compared with satellite
243 data. A summary of the observational data from surface networks and satellite retrievals can be
244 found in Table S3. The variables that are analyzed in this study include O₃, particulate matter with
245 diameter less than and equal to 2.5 and 10 μm (PM_{2.5} and PM₁₀, respectively), and PM_{2.5} species
246 including sulfate (SO₄²⁻), ammonium (NH₄⁺), nitrate (NO₃⁻), EC, OC, and total carbon (TC = EC
247 + OC), temperature at 2-m (T2), relative humidity at 2-m (RH2), and wind speed at 10-m (WS10),
248 wind direction at 10-m (WD10), precipitation, aerosol optical depth (AOD), cloud fraction
249 (CLDFRA), cloud water path (CWP), cloud optical thickness (COT), CDNC, cloud condensation
250 nuclei (CCN), downward shortwave radiation (SWDOWN), net shortwave radiation (GSW),

251 downward longwave radiation (GLW), outgoing longwave radiation at the top of atmosphere
252 (OLR), and shortwave and longwave cloud forcing (SWCF and LWCF). While uncertainties exist
253 in all the observational data used, systematic uncertainty analysis/quantification is beyond the
254 scope of this work. In this work, all observational data are considered to be the true values in
255 calculating the performance statistics. The information on the accuracy of most data used in the
256 model evaluation has been provided in Table 2 of Zhang et al. (2012a). Uncertainties associated
257 with some of the observational data are discussed in Section 3.

258 **3. Model Performance Evaluation**

259 **3.1 Meteorological Predictions**

260 Table 2 summarizes the statistics for T2, RH2, WS10, WD10, and precipitation. The model
261 performs very well for a 10-year average T2 with a slight underprediction (an MB of -0.3 °C).
262 This is better or consistent with other studies which tend to report underpredictions in simulated
263 T2. Brunner et al. (2014) reported a range of monthly MBs for T2 of -2 to 1 °C for simulations
264 using a number of CTMs over individual years for 2006 and 2010 with reanalysis meteorological
265 ICs/BCs. Seasonal temperature biases of -1.8 to -2.3 °C were reported from an ensemble of
266 regional climate models (RCMs) for a simulation period of 1971 to 2000 over northeastern U.S.
267 (Rawlins et al., 2012). He et al. (2015) also showed biases of -3 to 0 °C over CONUS when
268 compared against NCEP reanalysis data. Kim et al. (2013) compared the results of a number of
269 RCMs over CONUS over a climatological period of 1980 to 2003 against Climatic Research Unit
270 (CRU) surface analysis data at a 0.5° resolution and reported T2 biases of -5 to 5 °C. Figure 9.2
271 from Flato et al. (2013) shows that the Coupled Model Intercomparison Project Phase 5 (CMIP5)
272 models tend to underpredict T2 for the period of 1980 to 2005 over western U.S. by up to -3 °C.
273 The slight bias in T2 can be attributed to errors in soil temperature and soil moisture (Pleim and

274 Gilliam, 2009) or errors in the green vegetation fraction in the National Center for Environmental
275 Prediction, Oregon State University, Air Force and Hydrologic Research Lab (NOAH) Land
276 Surface Model (LSM) (Refslund et al., 2013). RH2 and WS10 are slightly overpredicted.
277 Precipitation is largely overpredicted, consistent with overpredictions in precipitation from WRF
278 and WRF/Chem simulations reported in literatures. For example, Caldwell et al. (2009) attributed
279 the overprediction in precipitation to overprediction in precipitation intensity but underprediction
280 in precipitation frequency. Otte et al. (2012) also reported that the precipitation predicted by WRF
281 is too high compared to the North American Regional Reanalyses (NARR) data throughout the
282 whole CONUS domain over a period of 1988 – 2007. Nudging and reinitialization have been most
283 commonly used methods to control such errors. . Three sensitivity simulations are conducted for
284 a summer month (July 2005) to pinpoint likely causes of the precipitation biases. The baseline
285 simulation (**Base**) uses a monthly reinitialization frequency, CESM_NCSU ICs/BCs, and the Grell
286 3D cumulus parameterization. The sensitivity simulations include (1) **Sen1**, which is similar to the
287 Base case except with a 5-day reinitialization period; (2) **Sen2**, which is similar to Base except
288 using NCEP for the meteorological ICs/BCs; and (3) **Sen3**, which is similar to Base except using
289 WRF/Chem v3.7 with the Multi-Scale Kain Fritsch (MSKF) cumulus parameterization, instead
290 of Grell 3D. The differences in configuration setup in those sensitivity simulations are given in
291 Table S4. The evaluation and comparison of the baseline and sensitivity results in July 2005 are
292 summarized in Tables S5 and S6, and Figure S1 in the supplementary material. As shown in Tables
293 S5-S6 and Figure S1, the precipitation bias can be attributed to several factors including the use of
294 Grell 3D cumulus parameterization scheme, the use of bias-corrected CESM_NCSU data (instead
295 of NCEP reanalysis data), and the use of an reinitialization frequency of 1-month, among which
296 the first factor dominates the biases in precipitation predictions. The simulated precipitation is

297 very sensitivity to different cumulus parameterizations. Compared to scale-aware
298 parameterizations such as the multi-scale Kain-Fritsch (MSKF) cumulus scheme, the Grell 3D
299 parameterization has a tendency to overpredict precipitation, particularly over ocean.

300 Figure 1 shows the spatial distributions of MB for 10-year average predictions of T2, RH2,
301 WS10, and precipitation. Figure 2 shows the time series of 10-year average monthly and annual
302 average T2, WS10, RH2, precipitation, O₃, and PM_{2.5} against observational data and IOA statistics.
303 T2 (Figure 1a) tends to be underpredicted over eastern and western U.S. and overpredicted over
304 the central U.S. The bias correction method itself may also contribute to the slight biases in T2. A
305 single temporally averaged (2001 – 2010) NCEP reanalysis file is applied to the 6-hourly BCs for
306 each individual year, which would in some cases contribute to the biases in the climatological 10-
307 year evaluation. T2 also tends to be overpredicted during the cooler months but underpredicted
308 during the warmer months (Figure 2a). While the bar charts in Figure 2 show domain- average
309 mean observed and mean simulated T2, IOA performance takes into account the proportion of
310 differences between mean observed and mean simulated values at different sites.

311 The model performance in terms of IOA for T2 is slightly worse during the warmer months
312 as compared to the cooler months; however, IOA values for all months are ≥ 0.9 . The poorer IOA
313 statistics for the warmer months are possibly influenced to a certain extent by the fact that the IOA
314 tends to be more sensitive towards extreme values (when temperatures are maximum) due to the
315 squared differences used in calculating IOA (Legates and McCabe, 1999). As shown in Figures 1b
316 and 2b, the spatial distributions of MBs for RH2 follow closely the spatial distributions of MBs
317 for T2, where T2 is underpredicted, RH2 is overpredicted and vice versa. Unlike T2, the IOA for
318 RH2 is the highest during the warmer months and the lowest during the winter months, but IOA
319 for RH2 is generally high (> 0.7) for all months. WS10 is also generally overpredicted along the

320 coast, over eastern U.S. and some portions over the western U.S. (Figure 1c), consistent with
321 overpredictions of T2 over the coast, and partially due to unresolved topographical features. In this
322 case the topographic correction for surface winds used to represent extra drag from sub-grid
323 topography (Jimenez and Dudhia, 2012) is used as an option in the 10-yr WRF/Chem simulations;
324 however, WS10 is still overpredicted except for the areas of flat undulating land in the central U.S.
325 Jimenez and Dudhia (2012) also suggested that the grid points nearest to the observational data
326 might not be the most appropriate or most representative, and that the selection of nearby grid
327 points can help to reduce errors in surface wind speed estimations. In this study, as the evaluation
328 is conducted over the whole CONUS, the nearest grid points are used for evaluation, which could
329 also result in errors in wind speed evaluation. The positive T2 and WS10 bias along the coast could
330 be due to the fact that the model grids for temperatures and wind speeds are located over the ocean,
331 however, the observation points are located slightly inland. As shown in Figure 2, WS10 performs
332 well on average for the months of April, May, and June, and is overpredicted for the other months.
333 Nonetheless the climatological NMB for WS10 overall is low at 7.7% (Table 2). WS10 has higher
334 IOA values during the spring months and the lowest IOA during the summer months and in
335 November. The model performs relatively well in predicting WD10 variability with a Corr of 0.6,
336 indicating overall a more southerly direction domain-wide predicted by the model compared to
337 observations. Precipitation is overpredicted for all months except for June, especially during the
338 summer months of July to August. Even with the inclusion of radiative feedback effects from the
339 subgrid-scale clouds in the radiation calculations, precipitation is still overpredicted with the Grell
340 3D scheme, which is consistent with the results shown by Alapaty et al. (2012). Precipitation
341 mainly has lower IOAs during the summer compared to other months, except in June which
342 actually exhibits the largest IOA of all months. Even though June is considered a summer month,

343 it does not show overprediction in precipitation compared to the other summer months. It is
344 possible that in June, the overall atmospheric moisture content is low. This is consistent with
345 simulated RH2 as June is the only month where RH2 is underpredicted compared to observations.

346 In general the model is able to reproduce the monthly trends in meteorological variables;
347 for example, the predicted trend in T2 closely follows the observed trends by NCDC. The observed
348 RH2 decreases from January to a minimum in April, and then increases from April to December.
349 Although the model predicts a similar pattern in RH2, there is a lag in the RH2 minimum occurring
350 two months later in June (Figure 2b). For WS10, the observation peaks in April, as compared to
351 the simulated peak in March. The model correctly predicts the observed WS10 minimum occurring
352 in August. The model trend in precipitation is similar to observations, except during the summer
353 months of July through September, where a large overprediction leads to a sharp increase in July,
354 followed by a gradual decrease through December.

355 Figures 2e – 2h show the annual time series trends for T2, RH2, WS10, and precipitation.
356 The model performs relatively well in predicting the annual mean T2 for most years (with MBs of
357 < 0.5 °C; Figure 2e). T2 also does not show an obvious decreasing or increasing T2 trend between
358 2001 and 2010. The IOA for annual T2 for all years are > 0.95 . However for 2002, mean simulated
359 T2 is ~ 0.7 °C higher than the observational data. IOA is still high for 2002 which indicates
360 probably good performance of T2 at most sites, however with large overpredictions at a few sites
361 which could skew the mean observed and mean simulated value but not influence IOA
362 significantly. RH2 is consistently overpredicted by the model with the largest overprediction in
363 2009. With the exception of 2009, observed RH2 is rather steady (65 – 70 %) from 2001 to 2010.
364 IOA is also steady for RH2, except for 2009. As mentioned earlier, WRF tends to overpredict
365 WS10 in general. Figure 2g shows that observations indicate weaker wind speeds from 2001 to

366 2007. Model performance is better from 2007 to 2010 with higher IOAs compared to previous
367 years. WRF has worse performance especially at weaker wind speeds as is the case from 2001 to
368 2007. Model performance for precipitation is more variable year-to-year, with IOAs ranging from
369 0.4 to 0.7; however, there is a systematic positive bias during the 10 year period.

370 Figure 3 shows the probability distribution functions (PDFs) of T2, RH2, WS10, and
371 precipitation against NCDC and NADP for 10 years. The observed and simulated variables are
372 averaged at each site for the 10-year period, and the pairs are then distributed into a PDF over 30
373 bins of observed and simulated values of T2. For T2, the simulated and observed PDFs are very
374 similar (Figure 3a), consistent with the statistics for T2 which shows only a small cold bias. The
375 model overpredicts T2 at sites where temperatures are very low. The PDF for simulated RH2 is
376 also shifted to the right of the observed RH2 (Figure 3b), with an observed and modeled peak 74%
377 and 78% respectively. The PDF of the bulk of the simulated WS10 is narrower (between 2 and 6
378 m s^{-1}) compared to that of observed WS10 (between 1 and 7 m s^{-1}). The model thus overpredicts
379 when near-surface wind speeds are low, but underpredicts when wind speeds are very high. This
380 suggests that the surface drag parameterization is still insufficient to help predict low wind speeds;
381 however, it might have contributed to the reduction in the simulated moderately high wind speeds
382 (Mass, 2012) (In this case, between 4 to 6 m s^{-1}). There are also instances where the model predicts
383 extremely high wind speeds ($> 8 \text{ m s}^{-1}$), which are also not found in the observed data. The PDF
384 for simulated precipitation against NADP also shows a shift to the right (which extends beyond 60
385 mm), consistent with the statistics for overpredicted precipitation and also with the PDF of RH2.
386 Nasrollahi et al. (2012) examined 20 combinations of microphysics and cumulus parameterization
387 schemes available in WRF and found that most parameterization schemes overestimate the amount
388 of rainfall and the extent of high rainfall values. In this study, while Grell 3D Ensemble cumulus

389 parameterization contributes in part to the overpredictions of precipitation, most overpredictions
390 occur at high thresholds as shown in Figure 3 (d) and they are attributed to possible errors in the
391 Morrison two moment scheme because the overpredictions of non-convective precipitation
392 dominate the overpredictions of total precipitation.

393 **3.2 Chemical Predictions**

394 **3.2.1 Ozone**

395 Table 2 summarizes the statistics for major chemical species. The model overpredicts
396 hourly O₃ mixing ratios on average against the Aerometric Information Retrieval System (AIRS)
397 – Air Quality System (AQS) with an NMB of 9.7% and an NME of 22.4%, but underpredicts O₃
398 mixing ratios against the Clean Air Status and Trends Network (CASTNET) with an NMB of -
399 8.8% and an NME of 19.8%. The O₃ mixing ratios are overpredicted at AIRS-AQS sites for all
400 climatological months except for April and May (Figure 4a) but underpredicted at CASTNET sites
401 for all months except for October with the largest underpredictions occurring in April and May
402 where IOA statistics are the lowest (Figure 4b). IOA statistics for all climatological months range
403 from 0.5 to 0.6 for AIRS-AQS and from 0.4 to 0.9 for CASTNET. In general, IOA values tend to
404 be higher for CASTNET compared to AIRS-AQS during the fall and winter months of October to
405 March. The IOA values for AIRS-AQS are rather steady on average over the 12 months compared
406 to CASTNET. This can be attributed to the larger dataset of AIRS-AQS (> 1000 stations)
407 compared to CASTNET (< 100 stations), the high and low undulations in O₃ averages at the
408 CASTNET sites tend to be smoothed or averaged out in O₃ averages at the AIRS-AQS sites given
409 larger AIRS-AQS dataset. The observed data from AIRS-AQS and CASTNET also show the
410 highest monthly O₃ mixing ratios over April and May. This result is consistent with the findings
411 of Cooper et al. (2014), who reported the highest mass of tropospheric O₃ for the northern

412 hemisphere in April and May based on the Ozone Monitoring Instrument (OMI) measurements in
413 2004, which suggested that the column mass of O₃ is not necessarily proportional to nitrogen oxide
414 (NO_x) emissions that peak during the summer. In addition, Cooper et al. (2014) attributed a shift
415 in the seasonal O₃ cycle observed at many rural mid-latitude monitoring sites to emissions
416 reductions in the U.S. The same study also reported that the summertime O₃ mixing ratios were
417 lower in eastern U.S. between 2005 and 2010 when compared to previous years, while remaining
418 relatively constant in spring. Thus the summer O₃ maximum during 2001- 2004 was replaced by
419 a broad spring/summer peak in 2005 - 2010. Both the observed and simulated O₃ mixing ratios do
420 not decrease for AIRS-AQS and CASTNET from 2001 to 2010 (Figures 4e and 4f). This is
421 somewhat consistent with Cooper et al. (2014) which showed that surface and lower tropospheric
422 O₃ has a decreasing trend over eastern U.S. but an increasing trend over the western U.S. from
423 1990-1999 to 2010. The predicted annual average O₃ mixing ratios are consistent from 2001 to
424 2010, with overpredictions and IOAs of ~0.6 at the AIRS-AQS sites, and underpredictions and
425 IOAs of ~0.6 to 0.8 at the CASTNET sites.

426 Figure 5 shows the PDFs of maximum 1-hour and 8-hour O₃ mixing ratios against
427 CASTNET and AIRS-AQS. The PDF of the observed and simulated O₃ mixing ratios are very
428 similar. The model is able to simulate the range and probabilities of O₃ mixing ratios relatively
429 well at both CASTNET and AIRS-AQS sites. At the CASTNET sites as shown in Figures 5a and
430 b, the model accurately predicts the peak maximum 1-hour O₃ mixing ratio centered at ~45 to 50
431 ppb, and the peak maximum 8-hour O₃ mixing ratio at ~42.5 ppb. At the AIRS-AQS sites as shown
432 in Figures 5c and d, the predicted PDF is slightly shifted to the right of the observations for both
433 maximum 1-hour and 8-hour O₃ mixing ratios. It is also interesting to note that the PDFs for
434 CASTNET and AIRS-AQS are quite different. CASTNET has a more uniform and normal

435 distribution compared to AIRS-AQS. The distribution for CASTNET data is also shifted towards
436 lower O₃ mixing ratios. The differences are attributed to the nature of the sites' locations, where
437 the AIRS-AQS network includes a mixture of urban, suburban and rural sites, leading to a less-
438 uniform normal distribution of O₃ mixing ratios centered at relatively higher O₃ mixing ratios,
439 while the CASTNET network includes mostly rural sites that exhibit a low maximum 1-hour and
440 8-hour O₃ mixing ratios, thus leading to a more uniform normal distribution that is heavier towards
441 the lower O₃ mixing ratios.

442 Figure 6 shows the diurnal variation of O₃ concentrations and IOA statistics for the four
443 climatological seasons against CASTNET (Figures a to d) and AIRS-AQS (Figures e to h) (Winter
444 - January, February and December (JFD); Spring - March, April, and May (MAM); Summer -
445 June, July, and August (JJA); Fall - September, October, and November (SON). Figure 6a shows
446 that in more rural sites (CASTNET) in winter O₃ tends to be underpredicted during the morning
447 (01:00 – 09:00 local standard time (LST)) and evening hours (18:00 – 24:00 LST). However,
448 Figure 6b shows that in general for all AIRS-AQS sites including urban sites, O₃ is systematically
449 overpredicted for all hours of the day. The diurnal trends for CASTNET and AIRS-AQS are
450 completely opposite for winter. As CASTNET sites are located in areas where urban influences
451 are minimal, most of these sites are likely to be NO_x-limited sites (Campbell et al., 2014).
452 Underpredicted NO_x emissions in rural areas can lead to underpredictions in O₃ concentrations in
453 NO_x-limited areas. As shown in Figure 2a), T2 is generally overpredicted during the winter
454 months, which explains the overpredictions in O₃ for most sites against AIRS-AQS. As shown in
455 Figures 6a, b and c, for CASTNET, the diurnal variations of O₃ in MAM and JJA are similar to
456 that in JFD. As shown in Figure 6d, slight overpredictions during the daylight hours of 10:00 to
457 17:00 LST occur in SON at the CASTNET sites, however the trends are similar for morning and

458 evening hours as compared to the other seasons. Similar to SON at the CASTNET sites, for AIRS-
459 AQS sites, overpredictions during daylight hours occur in JJA and SON (Figures 6 g and h), and
460 also to a much lesser extent in MAM (Figure 6f). This is probably due to the overpredictions of
461 T2, which are the smallest during MAM compared to other months as shown in Figure 2a.

462 Figure 7 compares the spatial distributions of 10-year average of the predicted and
463 observed hourly O₃ mixing ratios. The O₃ mixing ratios tend to be underpredicted in eastern and
464 northeastern U.S., where most of the CASTNET sites are located (Figure 7a). This is consistent
465 with the diurnal trends from Figures 6a to d which also show underpredictions for CASTNET sites.
466 From Figure 1a, T2 is underpredicted on average over northeastern U.S., which results in
467 underpredictions in biogenic emissions in the rural areas from MEGAN2. This would in turn
468 reduce O₃ mixing ratios in VOC-limited areas. O₃ photochemical reactivities would also be
469 reduced due to reduced T2. O₃ mixing ratios are, however, overpredicted over northwestern U.S.,
470 and also near the coastline of western U.S. The overprediction of O₃ mixing ratios in northwestern
471 U.S. can be attributed to an overprediction in the chemical BCs from CESM, as indicated by the
472 high O₃ mixing ratios near the northwestern region of the domain boundary.

473 **3.2.2 Particulate Matter**

474 The 10-year average PM_{2.5} concentrations are overpredicted with an NMB of 23.3 %
475 against IMPROVE, and underpredicted with an NMB of -10.8 % against the Speciated Trends
476 Network (STN) (Table 2). In addition, the IOA trend in Figure 4c shows very good performance
477 for PM_{2.5} against the Interagency Monitoring of Protected Visual Environments (IMPROVE) with
478 IOA values > 0.8. IOA values for PM_{2.5} against STN are high (~ 0.6 – 0.8) during the spring and
479 summer months, but lower (~ 0.4) during the winter months (Figure 4d). The IMPROVE surface
480 network covers generally rural areas and national parks while the STN surface network covers

481 urban sites. The horizontal resolution of $36 \times 36 \text{ km}^2$ used in this study may be too coarse to resolve
482 the locally high $\text{PM}_{2.5}$ concentrations at urban sites in STN which are in proximity of significant
483 point sources, especially during the fall and winter. During these colder seasons, $\text{PM}_{2.5}$
484 concentrations over the U.S. in general tend to be higher due to an extensive use of woodstove and
485 cold temperature inversions, which trap particulates near the ground (EPA, 2011). As shown in
486 Table 2, the concentrations of $\text{PM}_{2.5}$ species such as SO_4^{2-} , OC, and TC are overpredicted at the
487 IMPROVE sites, while the concentrations of the other main $\text{PM}_{2.5}$ species NO_3^- , NH_4^+ , and EC are
488 underpredicted at both IMPROVE and STN sites. TC concentrations, which are the sum of OC
489 and EC, are overpredicted due to larger overpredictions of OC compared to the underpredictions
490 of EC. The model also simulates both primary organic aerosol (POA) and secondary organic
491 aerosol (SOA). OC is calculated as the sum of POA and SOA divided by the ratio of OA/OC,
492 which is assumed to be a constant of 1.4 (Aitken et al., 2008). This calculation of OC using a
493 constant of 1.4 is an approximation, which is subject to uncertainties when comparing simulated
494 OC against observational data, as the ratio of OA/OC can be different in different environments
495 (Aitken et al., 2008).

496 As shown in Table 2, at the STN sites, the model slightly overpredicts the concentrations
497 of SO_4^{2-} , while underpredicting those of NO_3^- , NH_4^+ , and EC. The overpredictions of SO_4^{2-} are
498 likely due to the uncertainties that arise from processing of the RCP SO_2 emissions. The RCP SO_2
499 emissions are only available as a total emission flux, and they are not vertically distributed to the
500 important point sources such as furnaces and stacks. In this work, two steps are taken to resolve
501 the RCP elevated SO_2 emissions in each emission layer. First, a set of factors are derived from the
502 fraction of the elevated emissions in each layer to the vertical sum of emissions for NEI used by
503 default in the SMOKE model with the NEI data. Second, these factors are applied to the total RCP

504 emissions to obtain SO₂ emissions in each emission layer. The total RCP SO₂ emissions were
505 higher than the total NEI emissions, resulting in higher surface and elevated SO₂ emissions.
506 Figures 4g and 4h compare the modeled annual average time series for PM_{2.5} against IMPROVE
507 and STN observations, respectively. In general, the model performs well for PM_{2.5} at the
508 IMPROVE (IOA > 0.8) and STN (IOA ~ 0.5 – 0.7) sites. A declining trend in PM_{2.5} observed and
509 simulated concentrations are also observed over the years. For the later years (2007 to 2010), the
510 model performs significantly better against IMPROVE compared to STN. As 2010 NEI emissions
511 are used for the years 2007 to 2010, there are not many variations in the simulated PM_{2.5}
512 concentrations over these 4 years.

513 Figures 7 and 8 show the spatial plots of 10-yr average of simulated 24-hour average ,
514 PM₁₀, PM_{2.5}, and PM_{2.5} species concentrations, overlaid with observations from both STN and
515 IMPROVE. The underpredictions of PM₁₀ are dominated by an underprediction in the wind-blown
516 dust emissions, especially in western U.S. (Figure 7b). This is confirmed in Table 2, which shows
517 an MB of -11.5 μg m⁻³ and an NMB of -51.2% against PM₁₀ observations at AIRS-AQS sites. The
518 observational data indicate the elevated concentrations of dust over portions of Arizona and
519 California (> 50 μg m⁻³), which are not reproduced by the simulations (the simulated
520 concentrations are much lower, < 20 μg m⁻³). The AER/AFWA dust module (Table 1) does not
521 produce sufficient dust in this case, even though WS10 is overpredicted and is proportional to the
522 dust emissions. The sea-salt emission module by Gong et al. (1997), however, seems to produce a
523 reasonable amount of sea-salt as shown by the similar concentrations between simulated and
524 observational data for PM₁₀ near the coastlines. In addition, the MADE/VBS module in
525 WRF/Chem does not explicitly simulate the formation/volatilization of coarse inorganic species.

526 The coarse inorganic species are available, however, in the emissions and are transported and
527 deposited in a manner that is similar to non-reactive tracers.

528 The model performs well for $PM_{2.5}$ over eastern U.S. (Figure 7c), where modeled
529 concentrations are close to the observations; however, over the western U.S. there are
530 underpredictions in $PM_{2.5}$, especially in central to southern California. Even though Table 2 shows
531 in general an overprediction of SO_4^{2-} against STN sites, the model underpredicts SO_4^{2-} in regions
532 of elevated SO_4^{2-} concentrations, in particular, where concentrations are above $10 \mu\text{g m}^{-3}$ in the
533 vicinity of significant point sources of SO_2 and SO_4^{2-} over eastern U.S. (Figure 7d). This is likely
534 due to the coarse resolution ($0.5^\circ \times 0.5^\circ$) of RCP emissions, which probably results in a general
535 overprediction of SO_2 emissions over a grid but cannot resolve point sources smaller than the grid
536 resolution. A similar pattern is found for NH_4^+ over eastern U.S. due to underpredictions of high
537 concentrations of SO_4^{2-} (Figure 8a). There are also large underpredictions in NH_4^+ over the western
538 U.S. The underpredictions in NH_4^+ are likely due to underpredictions of NH_3 emissions from RCP.
539 The NH_3 emissions from RCP are much lower than those of NEI emissions over western U.S., by
540 more than a factor of 5, especially over portions of California. Large underpredictions occur over
541 both eastern and western U.S. for NO_3^- , EC, and TC (Figures 8b, c, and d). The underpredictions
542 in NO_3^- are more likely influenced by the underpredictions of NH_4^+ rather than NO_x emissions.
543 NO_x emissions for NEI are higher than those of RCP for a number of point sources, however, in
544 general RCP has higher NO_x emissions. Other possible reasons for the underpredictions of NO_3^-
545 concentrations include both prediction and measurement errors associated with SO_4^{2-} and TNH_4
546 that can greatly affect the performance of NO_3^- , inaccuracies in the assumptions used in the
547 thermodynamic model (e.g., the assumption that inorganic ions are internally mixed and the
548 equilibrium assumption might not be representative, especially for particles with larger diameters),

549 as well as inaccuracies in T2 and RH predictions (Yu et al., 2005). The statistics for IMPROVE
550 TC indicate overpredictions; however the statistics for STN TC indicate larger underpredictions
551 with an MB of $-2.0 \mu\text{g m}^{-3}$, which would explain the large underpredictions in $\text{PM}_{2.5}$ concentrations
552 over western U.S. The large underpredictions are in part impacted by uncertainties in emissions as
553 well as due to uncertainties in the precursor gas emissions for these species, especially for TC. The
554 RCP emissions of EC and POA are lower when compared to those of NEI. NEI emissions have a
555 higher spatial resolution, and thus more adequately represent the emissions from point sources
556 compared to RCP. The underpredictions of TC are also more likely due to underpredictions in EC
557 as compared to OC, as shown in underpredictions of EC by Figure 8c. As T2 is slightly
558 underpredicted, these could have resulted in underpredictions in isoprene and terpene, which are
559 major gas precursors of biogenic SOA, resulting in lower SOA and OC concentrations. In addition,
560 the emissions of anthropogenic VOC species from RCP which are also of a lower spatial resolution
561 compared to their emissions in the NEI tend to also be lower than NEI levels especially at point
562 sources. The underpredictions for these particulate species, especially for water-soluble species
563 including NH_4^+ and NO_3^- are also likely impacted by overpredictions in precipitation (Figure 2d),
564 which leads to an overprediction in their wet deposition rates and thus a reduction of their ambient
565 concentrations. The overpredictions in WS10 also help contribute to the deposition of $\text{PM}_{2.5}$ and
566 $\text{PM}_{2.5}$ species onto the ground (Sievering et al., 1987).

567 **3.3 Aerosol, Cloud, and Radiation Predictions**

568 There are uncertainties in the satellite retrievals of various aerosol-cloud-radiation
569 variables from the Clouds and the Earth's Radiant Energy System (CERES) and the Moderate
570 Resolution Imaging Spectroradiometer (MODIS). Loeb et al. (2009) reported that the major
571 uncertainties of the top of atmosphere radiative fluxes from CERES are derived from instrument

572 calibration (with a net error of 4.2 W m^{-2}), and the assumed value of 1 W m^{-2} for total solar
573 irradiance. However, there is good correlation ($R > 0.8$) between the model and CERES for the
574 radiation variables SWDOWN, GSW, and GLW, which are all measured at the surface (Table 2).
575 Modeled OLR at the top of the atmosphere also has relatively good correlation ($R \sim 0.6$).
576 SWDOWN and GLW are both slightly overpredicted due to influences from biases in PM
577 concentrations and clouds, but GSW and OLR are slightly underpredicted.

578 The overpredictions of the surface radiation variables are also impacted by the
579 underpredictions in AOD and COT. AOD is underpredicted with an NMB of -24.0%, and COT is
580 underpredicted with an NMB of -44.3%. These underpredictions indicate that less radiation is
581 attenuated (i.e., absorbed or scattered) or reflected while traversing through the atmospheric
582 column and clouds, thus allowing more radiation to reach the ground. Using the CESM model, He
583 et al. (2015) also showed underpredictions in AOD and COT over CONUS against MODIS
584 satellite retrievals. Figure 9 compares the spatial distributions of the 10-year average predictions
585 of AOD (a and b) against the satellite retrieval data from MODIS. The simulated AODs show
586 relatively large values over eastern U.S., due to the relatively higher PM concentrations in this
587 region of the U.S. The MODIS AOD, however, shows slightly elevated values over eastern U.S.,
588 but the magnitudes are not as high as the simulated AOD over eastern U.S. MODIS-derived AOD
589 is also higher over western U.S. compared to eastern U.S., and this trend is not found in the
590 simulated AOD. The differences between the MODIS AOD and the simulated AOD are likely due
591 to the differences in the algorithms used to retrieve AOD based on MODIS measurements and
592 calculate AOD in WRF/Chem. For MODIS, AOD is calculated by matching the spectral
593 reflectance observations with a lookup table based on a set of aerosol parameters including the
594 aerosol size distributions from a variety of aerosol models, which differ based on seasons and

595 locations (Levy et al., 2007). There are also different algorithms for dark land, bright land, and
596 over oceans (Levy et al., 2013). The MODIS data are aggregated into a global 1° gridded (Level-
597 3) dataset with monthly (MOD08_M3) temporal resolution
598 ([https://www.earthsystemcog.org/site_media/projects/obs4mips/TechNote_MODIS_L3_C5_Aer](https://www.earthsystemcog.org/site_media/projects/obs4mips/TechNote_MODIS_L3_C5_Aerosols.pdf)
599 [osols.pdf](https://www.earthsystemcog.org/site_media/projects/obs4mips/TechNote_MODIS_L3_C5_Aerosols.pdf)). The inaccuracies for the calculation of AOD in WRF/Chem include biases in aerosol
600 size distribution, aerosol composition, aerosol water content, and reflectances. They can also arise
601 from parameterizations in the calculations including the assumption of an internally-mixed aerosol
602 composition. Therefore, caution should also be taken when comparing simulated AOD with the
603 satellite-derived AOD products. Toth et al. (2013) compared Aqua MODIS AOD products over
604 the mid to high latitude Southern Ocean where a band of enhanced AOD is observed, to cloud and
605 aerosol products produced by the Cloud-Aerosol Lidar with Orthogonal Polarization (CALIOP)
606 project; and AOD data from the Aerosol Robotic Network (AERONET) and the Maritime Aerosol
607 Network (MAN). They concluded that the band of enhanced AOD is not detected in the CALIOP,
608 AERONET, or MAN products. The enhanced AOD band is attributed to stratocumulus and low
609 broken cumulus cloud contamination, as well as the misidentification of relatively warm cloud
610 tops compared with surrounding open seas.

611 Figure 9 also shows spatial distributions of the 10-year average predictions of CDNC (c
612 and d), CWP (e and f), and COT (g and h), compared against the satellite retrieval data from
613 MODIS. The cloud variables CDNC, CWP, and COT tend to be underpredicted for most of the
614 regions over the U.S. However, CWP is largely overpredicted over the Atlantic ocean. This is also
615 likely due to the build-up of moisture over the Atlantic ocean, also influencing precipitation as
616 mentioned previously. CDNC is overpredicted over some regions in eastern U.S., but there are
617 also relatively large areas of underpredictions over both the land and ocean. This leads to an

618 average domain-wide underprediction for CDNC (Table 2). This is likely due to the differences in
619 deriving CDNC in the model and in the satellite retrievals. CDNC in the model is calculated based
620 on the activation parameterization by Abdul Razzak and Ghan (2000) based on the aerosol size
621 distribution, aerosol composition, and the updraft velocity. The MODIS-derived CDNC from
622 Bennartz (2007) is calculated based on cloud effective radius and COT, which would explain the
623 differences in spatial patterns between model and observed data. As indicated by Bennartz (2007),
624 the errors in CDNC can be up to 260%, especially for regions with low CF (< 0.1). The model and
625 MODIS spatial patterns are similar for CWP and COT over land, although the model values are
626 underpredicted. King et al. (2013) reported that the MODIS retrieval of cloud effective radius
627 when compared to in-situ observations is overestimated by 13% on average. Combined with
628 overestimations in COT, this leads to overestimation of liquid water path. In addition, there can
629 also be differences in satellite-derived cloud products from different satellites. For example, Shan
630 et al. (2011) showed that the derived CLDFRA from MODIS and another satellite, the Polarization
631 and Directionality of Earth Reflectances (POLDER) can differ with a global average of 10%.

632 Figure 10 shows similar spatial plots for modeled versus CERES derived SWDOWN,
633 OLR, SWCF, and LWCF. We note that modeled SWCF is calculated based on the differences
634 between the net cloudy sky and net clear sky shortwave radiation at the top of atmosphere, which
635 in turn are dependent on cloud properties including the CLDFRA, COT, cloud asymmetry
636 parameter, and cloud albedo. It is possible that due to the overprediction of CLDFRA, the
637 magnitudes of the simulated SWCF are greater than those from CERES (Figures 10c and 10g),
638 even though the other cloud variables are underpredicted. LWCF is calculated based on the
639 differences in clear-sky OLR and cloudy-sky OLR, which in turn are dependent on CLDFRA,
640 COT, and absorbance and radiance due to atmospheric gases. The underprediction of total-sky

641 OLR (Table 2 and Figures 10b and 10f) leads to an overprediction in LWCF. SWCF is largely
642 overpredicted over eastern U.S. and especially over the Atlantic ocean (Figures 10c and 10g).
643 LWCF is also overpredicted by the model in similar locations as SWCF, such as in southeastern
644 U.S., and over the ocean in the eastern portion of the domain (Figures 10d and 10h). This is further
645 confirmed by the underpredictions in SWDOWN over the Atlantic ocean and in general over the
646 eastern portion of the domain, as increased clouds (as a consequence of overpredicted AOD, CWP
647 and COT) and SWCF lead to less SWDOWN reaching the ground (Figures 10a and 10e) which
648 also eventually leads to a reduction in the OLR also over the eastern portion of the domain. The
649 larger negative SWCF and positive LWCF in the model compared to CERES, however, lead to an
650 overall good agreement with CERES for the net cloud forcing (SWCF + LWCF; not shown). The
651 mean bias for SWCF against CERES of 7.8 W m^{-2} and that for LWCF against CERES of 6.9 W
652 m^{-2} are comparable to the results from the CMIP5 models of -10 to 10 W m^{-2} over CONUS region
653 (Figure 9.5 in Flato et al., 2013). The evaluation of 10-year averaged predictions of aerosol-cloud-
654 radiation variables is similar to the results from the WRF/Chem simulations in 2006 and 2010 by
655 Yahya et al. (2014 and 2015). For example WRF/Chem generally performs well for cloud fraction
656 but AOD, CDNC, CWP and COT are underpredicted in both studies, which possibly indicate
657 consistent biases for every year contributing to climatological biases.

658 **4. Summary and Conclusions**

659 Overall, the model slightly underpredicts T2 with a mean bias of $\sim -0.3 \text{ }^\circ\text{C}$, which is
660 consistent or better than other studies based on chemical transport models and regional climate
661 models. The underpredictions in T2 correlate to the overpredictions in RH2. WS10 biases are
662 likely due to issues with unresolved topography or due to inaccuracies in the selection of
663 representative grid points. There are seasonal biases in precipitation, where overpredictions tend

664 to occur largely over the summer months; however, precipitation is overpredicted every year
665 between 2001 and 2010 likely due mainly to uncertainties in WRF cumulus and microphysics
666 parameterizations. In particular, the use of a different cumulus parameterization scheme, e.g.,
667 based on the MSKF available in WRF/Chem version 3.7 or newer has been shown in the sensitivity
668 study to significantly reduce precipitation biases. Other factors contributing to the precipitation
669 bias include the use of bias-corrected CESM_NCSU data (instead of NCEP reanalysis data), and
670 the use of an reinitialization frequency of 1-month. A satisfactory model performance for
671 meteorological variables is important and necessary when simulating future years, as data
672 evaluation is not possible. Meteorological variables such as temperature, humidity, wind speed
673 and direction, PBL height, and radiation have a strong impact on chemical predictions, and thus
674 are critical to the satisfactory model performance when predicting chemical variables such as O₃
675 and PM_{2.5}. Biases in O₃ and PM_{2.5} concentrations can be attributed to biases in any of the
676 meteorological and chemical variables. The model performs generally well for radiation variables,
677 as well as for the main chemical species such as O₃ and PM_{2.5}, which indicates that the processed
678 RCP 8.5 emissions are reasonably accurate to produce acceptable results for the concentrations of
679 chemical species.

680 Modeled O₃ mixing ratios at the CASTNET sites are slightly underpredicted, but are
681 slightly overpredicted at AIRS-AQS sites, in part due to the fact that the CASTNET sites are
682 classified as rural, while the AIRS-AQS sites are classified as both urban and rural. O₃ mixing
683 ratios at the AIRS-AQS sites tend to be overpredicted during the colder fall and winter seasons,
684 and annually, O₃ mixing ratios are overpredicted every year from 2001 to 2010. O₃ mixing ratios
685 at the CASTNET sites are underpredicted for all climatological months, while the largest
686 underpredictions are observed from January to May. However, on a decadal time scale,

687 WRF/Chem adequately represents the different O₃ PDFs at the AIRS-AQS and CASTNET sites.
688 This study also showed that peak O₃ mixing ratios are observed over April and May rather than
689 June to August, which is consistent with Cooper et al. (2014) who attributed this to emission
690 reductions and opposite trends in O₃ mixing ratios over eastern and western U.S. over the last 20
691 years. Modeled PM_{2.5} concentrations tend to be overpredicted at the IMPROVE sites but
692 underpredicted at the STN sites. PM_{2.5} at the IMPROVE sites tend to be underpredicted in spring
693 and summer but overpredicted in fall and winter, while PM_{2.5} concentrations against STN are
694 persistently underpredicted for all climatological months. The IMPROVE and STN sites are
695 classified as rural and urban, respectively. Due to the relatively coarse horizontal resolution of the
696 model (36 × 36 km), the model is unable to capture the locally higher PM_{2.5} concentrations at the
697 STN sites. In general, however, the model performs relatively well for total PM_{2.5} concentrations
698 at the IMPROVE and STN sites with NMBs of within ±25%, although larger biases exist for PM_{2.5}
699 species. Model performance for PM₁₀ should be improved, as PM₁₀ also has important impacts on
700 climate through influencing the radiative budget both directly and indirectly due to its larger size
701 and higher concentrations. The choice of observational networks for model evaluation are
702 therefore important as both networks can show positive and negative biases depending on the type
703 and location of the sites (e.g., O₃ against AIRS-AQS and CASTNET, and PM_{2.5} against STN and
704 IMPROVE). The major uncertainties lie in the predictions of cloud-aerosol variables. As
705 demonstrated in this study, large biases and error in simulating cloud variables even in the most
706 advanced models such as WRF/Chem, indicating a need for future improvement in relevant model
707 treatments such as cloud dynamics and thermodynamics, as well as aerosol-cloud interactions. In
708 addition, there are large uncertainties in satellite retrievals of cloud variables for evaluation. In this
709 study, most of the cloud-aerosol variables including AOD, COT, CWP, and CDNC are on average

710 underpredicted across the domain; however, the overpredictions of cloud variables including COT
711 and CWP over the Atlantic ocean and eastern U.S. lead to underpredictions in radiation and
712 overpredictions in cloud forcing, which are important parameters when simulating future climate
713 change.

714 In summary, the model is able to predict O₃ mixing ratios and PM_{2.5} concentrations
715 relatively well with regards to decadal scale air quality and climate applications. The model is able
716 to predict meteorological variables satisfactorily and with results comparable to RCM and GCM
717 applications from literatures. Possible reasons behind the chemical and meteorological biases
718 identified through this work should be taken into account when simulating longer climatological
719 periods and/or future years. Aerosol-cloud-radiation variables are important for climate
720 simulations, the performance of these variables are not as good as that of the chemical and
721 meteorological variables. They contain consistent biases in single-year evaluations of WRF/Chem.
722 However, magnitudes of biases for SWCF and LWCF are comparable to those from literature,
723 which suggests that model improvements should be made in terms of bias correction of
724 downscaled ICs/BCs as well as aerosol-cloud-radiation parameterizations in the model. In
725 addition, having consistent physical and chemical mechanisms between the GCM and RCMs could
726 help to reduce uncertainties in the results (Ma et al., 2014). Although CESM and WRF/Chem use
727 similar chemistry and aerosol treatments in this work, they use somewhat different physics
728 schemes which may contribute to such uncertainties. The development of scale-aware
729 parameterizations that can be applied at both global and regional scales would help reduce
730 uncertainties associated with the use of different schemes for global simulations and downscaled
731 regional simulations.

732

733 **Code and Data Availability**

734 The WRF/Chem v3.6.1 code used in this paper will be available upon request. However,
735 we highly encourage users to download the latest available version of the WRF/Chem code from
736 NOAA's web site at http://www2.mmm.ucar.edu/wrf/users/download/get_source.html. The
737 updates in our in-house version of WRF/Chem v3.6.1 has been implemented into WRF/Chem
738 v3.7 and WRF/Chem v3.7.1 for scientific community release. The WRF/Chem v3.7 and
739 WRF/Chem v3.7.1 codes are now publicly available at
740 http://www2.mmm.ucar.edu/wrf/users/download/get_source.html. These latest versions of the
741 source codes contain all major changes in the standard version of WRF/Chem v3.6.1 used in for
742 this study. In addition, they have been rigorously tested for compatibility and compiling issues
743 on various platforms. The inputs including the meteorological files, meteorological initial and
744 boundary conditions, chemical initial and boundary conditions, model set-up and configuration,
745 and the namelist set-up, and instructions on how to run the simulations for a 1-day test case, as
746 well as a sample output for 1-day test can be provided upon request.

747 **Acknowledgments**

748 This study is funded by the National Science Foundation EaSM program (AGS-1049200) at
749 NCSU. The emissions for chemical species that are not available from the RCP emissions are
750 taken from the 2008 NEI-derived emissions for 2006 and 2010 provided by the U.S. EPA,
751 Environment Canada, and Mexican Secretariat of the Environment and Natural Resources
752 (Secretaría de Medio Ambiente y Recursos Naturales-SEMARNAT) and National Institute of
753 Ecology (Instituto Nacional de Ecología-INE) as part of the Air Quality Model Evaluation
754 International Initiative (AQMEII). The hourly temporal profiles of 2001, 2005, and 2010 RCP
755 emissions are based on the 2002NEI and the AQMEII 2006 and 2010 emissions derived based on

756 the 2008 NEI. The authors acknowledge use of the WRF-Chem preprocessor tool mozbc provided
757 by the Atmospheric Chemistry Observations and Modeling Lab (ACOM) of NCAR and the script
758 to generate initial and boundary conditions for WRF based on CESM results provided by Ruby
759 Leung, PNNL. For WRF/Chem simulations, we would like to acknowledge high-performance
760 computing support from Yellowstone (ark:/85065/d7wd3xhc) provided by NCAR's
761 Computational and Information Systems Laboratory, sponsored by the National Science
762 Foundation.

763

764 **References**

765 Abdul-Razzak, H. and Ghan, S. J.: A parameterization of aerosol activation, 2. Multiple aerosol
766 types, *J. Geophys. Res.*, 105(5), 6837-6844, 2000.

767 Aitken, A.C., DeCarlo, P.F., Kroll, J.H., Worsnop, D.R., Huffman, J.A., Docherty, K.S., Ulbrich,
768 I.M., Mohr, C., Kimmel, J.R., Sueper, D., Sun, Y., Zhang, Q., Trimborn, A., Northway, M.,
769 Ziemann, P.J., Canagaratna, M.R., Onasch, T.B., Alfarra, M.R., Prevot, A.S.H., Dommen, J.,
770 Duplissy, J., Metzger, A., Baltensperger, U. and Jimenez, J.L.: O/C and OM/OC ratios of
771 primary, secondary and ambient organic aerosols with high-resolution time of flight aerosol
772 mass spectrometry, *Environ. Sci. Technol.*, 42, 4478 – 4485, 2008.

773 Alapaty, K., Herwehe, J., Nolte, C.G., Bullock, R.O., Otte, T.L., Mallard, M.S., Dudhia, J. and
774 Kain, J.S.: Introducing subgrid-scale cloud feedbacks to radiation in WRF, the 13th WRF Users
775 Workshop, Boulder, CO, June 26 to 29, 2012.

776 Ahmadov, R., McKeen, S.A., Robinson, A.L., Bareini, R., Middlebrook, A.M., De Gouw, J.A.,
777 Meagher, J., Hsie, E.-Y., Edgerton, E., Shaw, S. and Trainer, M.: A volatility basis set model

778 for summertime secondary organic aerosols over the eastern United States in 2006, J.
779 Geophys. Res. 117, D06301, doi:10.1029/2011JD016831, 2012.

780 Beniston, M., Stephenson, D.B., Christensen, O.B., Ferro, C.A.T., Frei, C., Goyette, S.,
781 Halsnaes, K., Holt, T., Jylha, K., Koffi, B., Palutikof, J., Scholl, R., Semmler, T. and Woth,
782 K.: Future extreme events in European climate: an exploration of regional climate model
783 projections, *Clim. Change*, 81, 71 – 95, doi: 10.1007/s10584-006-9226-z, 2007.

784 Bennartz, R.: Global assessment of marine boundary layer cloud droplet number concentration
785 from satellite, *J. Geophys. Res-Atmos*, 112(D2), D02201, doi:10.1029/2006JD007547, 2007.

786 Brunner, D., Savage, N., Jorba, O., Eder, B., Giordano, L., Badia, A., Balzarini, A., Baro, R.,
787 Bianconi, R., Chemel, C., Curci, G., Forkel, R., Jimenez-Guerrero, P., Hirtl, M., Hodzic, A.,
788 Hozak, L., Im, U., Knote, C., Makar, P., Manders-Groot, A., van Meijgaard, E., Neal, L.,
789 Perez, J.L., Pirovano, G., San Jose, R., Schroder, W., Sokhi, R.S., Syrakov, D., Torian, A.,
790 Tuccella, P., Werhahn, J., Wolke, R., Yahya, K., Zabkar, R., Zhang, Y., Hogrefe, C. and
791 Galmarini, S.: Comparative analysis of meteorological performance of coupled chemistry-
792 meteorology models in the context of AQMEII phase 2, *Atmos. Environ.*, in press,
793 doi:10.1016/j.atmosenv.2014.12.032, 2014.

794 Caldwell, P., H.-N.S. Chin, D.C. Bader, and G. Bala (2009), Evaluation of a WRF dynamical
795 downscaling simulation over California, *Clim. Change.*, 95, 499-521.

796 Campbell, P. C., Zhang, Y., Yahya, K., Wang, K., Hogrefe, C., Pouliot, G., Knote, C., Hodzic,
797 A., San Jose, R., Perez, J., Jimenez-Guerrero, P., Baro, R. and Makar, P.: A Multi-Model
798 Assessment for the 2006 and 2010 Simulations under the Air Quality Model Evaluation
799 International Initiative (AQMEII) Phase 2 over North America: Part I, Indicators of the

800 Sensitivity of O₃ and PM_{2.5} Formation Regimes, Atmos. Environ., in press,
801 doi:10.1016/j.atmosenv.2014.12.026, 2014.

802 Chen, F. and Dudhia, J.: Coupling an advanced land-surface/hydrology model with the Penn
803 State/NCAR MM5 modeling system. Part I: Model implementation and sensitivity. Mon.
804 Wea. Rev., 129, 569-585, 2001.

805 Clough, S.A., Shephard, M.W., Mlawer, J.E., Delamere, J.S., Iacono, M.J., Cady-Pereira, K.,
806 Boukabara, S. and Brown, P.D.: Atmospheric radiative transfer modeling: a summary of the
807 AER codes, J. Quant. Spectrosc. Radiat. Transfer, 91(2), 233 – 244, doi:
808 10.1016/j.qsrt.2004.05.058, 2005.

809 Cooper, O.R., Parrish, D.D., Ziemke, J., Balashov, N.V., Cupeiro, M., Galbally, I.E., Gilge, S.,
810 Horowitz, L., Jensen, N.R., Lamarque, J.-F., Naik, V., Oltmans, S.J., Schwab, J., Shindell,
811 D.T., Thompson, A.M., Thouret, V., Wang, Y. and Zbinden, R.M.: Global distribution and
812 trends of tropospheric ozone: An observation-based review, Elem. Sci. Anth., 2, 000029,
813 doi:10.12952/journal.elementa.000029, 2014.

814 Dasari, H.P., Salgado, R., Perdigo, J. and Challa, V.S.: A regional climate simulation study
815 using WRF-ARW model over Europe and evaluation for extreme temperature weather
816 events, Intl. J. of Atmos. Sci., ID 704079, doi:10.1155/2014/704079, 2014.

817 Ek, M.B., Mitchell, K.E., Lin, Y., Rogers, E., Grunmann, P., Koren, V., Gayno, G. and Tarpley,
818 J.D.: Implementation of NOAA land surface model advances in the National Centers for
819 Environmental Prediction operational mesoscale model, J. Geophys. Res., 108, D22, 8851,
820 doi:10.1029/2002JD003296, 2003.

821 EPA.: Our Nation's Air – Status and Trends through 2010, Particle Pollution, Report by the U.S.
822 EPA, 4pp, <http://www.epa.gov/airtrends/2011>, 2011, last accessed July 6th, 2015.

823 Fan, F., Bradley, R.S. and Rawlins, M.A.: Climate change in the northeastern U.S.: regional
824 climate validation and climate change projections, *Clim. Dyn.*, 43, 145 – 161,
825 doi:10.1007/s00382-014-2198-1, 2014.

826 Feser, F., Rockel, B., Von Storch, H., Winterfeldt, J. and Zahn, M.: Regional climate models add
827 value to global model data, *Bull. Amer. Meteor. Soc.*, 92, 1181 – 1192, 2011.

828 Flato et al.: Evaluation of Climate Models, In: *Climate Change 2013: The Physical Science*
829 *Basis. Contribution of Working Group I to the Fifth Assessment Report of the*
830 *Intergovernmental Panel on Climate Change* [Stocker, T.F., D. Qin, G.-K. Plattner, M.
831 Tignor, S.K. Allen, J. Boschung, A. Nauels, Y. Xia, V. Bex and P.M. Midgley (eds.)],
832 Cambridge University Press, Cambridge, United Kingdom and New York, NY, U.S.A.,
833 2013.

834 Gao, Y., Fu, J.S., Drake, J.B., Liu, Y. and Lamarque, J.F.: Projected changes of extreme weather
835 events in the eastern United States based on a high resolution climate modeling system,
836 *Environ. Res. Lett.*, 7, 044025, 2012.

837 Gao, Y., Fu, J.S., Drake, J.B., Lamarque, J.-F. and Liu, Y.: The impact of emission and climate
838 change on ozone in the United States under representative concentration pathways (RCPs),
839 *Atmos. Chem. Phys.*, 2013, 9607 – 9621, 2013.

840 Glotfelty, T., He, J. and Zhang, Y.: Updated organic aerosol treatments in CESM/CAM5:
841 development and initial application, in preparation, 2015.

842 Gong, S., Barrie, L.A. and Blanchet, J.P.: Modeling sea salt aerosols in the atmosphere: 1. Model
843 development, *J. Geophys. Res.*, 102, 3805-3818, doi:10.1029/96JD02953, 1997.

844 Grell, G.A., Knoche, R., Peckham, S.E. and McKeen, S.A.: Online versus offline air quality
845 modeling on cloud-resolving time scales, *Geophys. Res. Lett.*, 31 (16),
846 doi:10.1029/2004GL020175, 2004.

847 Grell, G.A., Peckham, S.E., Schmitz, R., McKeen, S.A., Frost, G., Skamarock, W.C. and Eder,
848 B.: Fully coupled “online” chemistry within the WRF model, *Atmos. Environ.*, 39, 6957-
849 6975, 2005.

850 Grell, G.A. and Freitas, S.R.: A scale and aerosol aware stochastic convective parameterization
851 for weather and air quality modeling, *Atmos. Chem. Phys.*, 14, 5233-5250, doi:10.5914/acp-
852 14-5233-2014, 2014.

853 Guenther, A., Kart, T., Harley, P., Wiedinmyer, C., Palmer, P.I. and Geron, C.: Estimates of
854 global terrestrial isoprene emissions using MEGAN (Model of Emissions of Gases and
855 Aerosols from Nature), *Atmos. Chem. Phys.*, 6, 3181-3210, 2006.

856 He, J., Zhang, Y., Glotfelty, T., He, R., Bennartz, R., Rausch, J. and Sartelet, K.: Decadal
857 simulation and comprehensive evaluation of CESM/CAM5.1 with advanced chemistry,
858 aerosol microphysics and aerosol-cloud interactions, *J. Adv. Model. Earth Syst.*, 7, 110 –
859 141, doi:10.1002/2014MS000360, 2015.

860 Hong, S.-Y., Noh, Y. and Dudhia, J.: A new vertical diffusion package with an explicit treatment
861 of entrainment processes, *Mon. Wea. Rev.*, 134, 2318-2341, 2006.

862 Hong, S.-Y.: A new stable boundary-layer mixing scheme and its impact on the simulated East
863 Asian summer monsoon, *Q.J.R. Meteorol. Soc.*, 136, 1481 – 1496, doi:0.1002/qj.665, 2010.

864 Hurrell, J.W., Holland, M.M., Gent, P.R., Ghan, S., Kay, J.E., Kushner, P.J., Lamarque, J.-F.,
865 Large, W.G., Lawrence, D., Lindsay, K., Lipscomb, W.H., Long, M.C., Mahowald, N.,
866 Marsh, D.R., Neale, R.B., Rasch, P., Vavrus, S., Vertenstein, M., Bader, D., Collins, W.D.,

867 Hack, J.J., Kiehl, J. and Marshall, S.: The Community Earth System Model: A framework for
868 collaborative research, *Bull. Am. Meteorol. Soc.*, 94, 1339 – 1360, doi:10.1175/BAMS-D-
869 12-00121.1, 2013.

870 Iacono, M.J., Delamere, J.S., Mlawer, E.J., Shepard, M.W., Clough, S.A. and Collins, W.D.:
871 Radiative forcing by long-lived greenhouse gases: Calculations with the AER radiative
872 transfer models, *J. Geophys. Res.*, 113, D13103, doi:10.1029/2008JD009944, 2008.

873 IPCC : Climate change 2013: the physical science basis. In: Stocker, T.F., Qin, D., Plattner, G.-
874 K., Tignor, M.M.B., Allen, S.K., Boschung, J., Nauels, A., Xia, Y., Bex, V., Midgley, P.M.
875 (Eds.), *Contribution of Working Group I to the Fifth Assessment Report of the*
876 *Intergovernmental Panel on Climate Change, Summary for Policymakers*, 2013.

877 Jacob, D., Barring, L., Christensen, O.B., Christensen, J.H., de Castro, M., Deque, M., Giorgi, F.,
878 Hagemann, S., Hirschi, M., Jones, R., Kjellstrom, E., Lenderink, G., Rockel, B., Sanchez, E.,
879 Schar, C., Seneviratne, S.I., Somot, S., van Ulden, A. and van den Hurk, B.: An inter-
880 comparison of regional climate models for Europe: model performance in present-day
881 climate, *Clim. Change*, 81, 31 – 52, 2007.

882 Jimenez, P.A. and Dudhia, J.: Improving the representation of resolved and unresolved
883 topographic effects on surface wind in the WRF model, *J. Appl. Meteor. Climatol.*, 51, 300 –
884 316, 2012.

885 Jones, R.G., Noguer, M., Hassell, D.C., Hudson, D., Wilson, S.S., Jenkins G.J. and Mitchell,
886 J.F.B.: *Generating high resolution climate change scenarios using PRECIS*, Met Office
887 Hadley Centre, Exeter, UK, 40 pp., April 2004, 2004.

888 Jones, S. and Creighton, G.: *AFWA dust emission scheme for WRF/Chem-GOCART*, 2011
889 WRF workshop, June 20-24, Boulder, CO, USA, 2011.

890 Karamchandani, P., Zhang, Y., Chen, S.-Y., and Balmori-Bronson, R.: Development of an
891 extended chemical mechanism for global-through-urban applications, *Atmos. Poll. Res.*, 3, 1
892 – 24, doi:10.5094/apr.2011.047.

893 Kim, J., Waliser, D.E., Mattmann, C.A., Mearns, L.O., Goodale, C.E., Hart, A.F., Crichton,
894 D.J., McGinnis, S., Lee, H., Loikith, P.C. and Boustani, M.: Evaluation of the surface
895 climatology over the conterminous United States in the North American Regional Climate
896 Change Assessment Program Hindcast Experiment using a regional climate model evaluation
897 system, *J. Climate*, 26, 5698 – 5715, 2013.

898 King, N.J., Bower, K.N., Crosier, J. and Crawford, I.: Evaluating MODIS cloud retrievals with in
899 situ observations from VOCALS-REx, *Atmos. Chem. Phys.*, 13, 191 – 209, 2013.

900 Legates, D.R. and McCabe Jr., G.J.: Evaluating the use of “goodness-of-fit” measures in
901 hydrologic and hydroclimatic model validation, *Water Resour. Res.*, 35(1), 233 – 241,
902 doi:10.1029/1998WR900018, 1999.

903 Levy, R.C., Remer, L.A. and Dubovik, O.: Global aerosol optical properties and application to
904 Moderate Resolution Imaging Spectroradiometer aerosol retrieval over land, *J. Geophys.*
905 *Res.*, 112(D13), doi:10.1029/2006JD007815, 2007.

906 Levy, R.C., Mattoo, S., Muchak, L.A., Remer, L.A., Sayer, A.M., Patadia, F., Hsu, N.C.: The
907 Collection 6 MODIS aerosol products over land and ocean, *Atmos. Meas. Tech.*, 6, 2989 –
908 3034, 2013.

909 Leung, R.L., Qian, Y. and Bian, X.: Hydroclimate of the Western United States based on
910 Observations and Regional Climate Simulation of 1981 – 2000, Part I: Seasonal Statistics, *J.*
911 *Clim.*, 16(12), 1892 – 1911, 2003.

912 Liu, X., Easter, R.C., Ghan, S.J., Zaveri, R., Rasch, P., Shi, X., Lamarque, J.-F., Gettelman, A.,
913 Morrison, H., Vitt, F., Conley, A., Park, S., Neale, R., Hannay, C., Ekman, A.M.L., Hess, P.,
914 Mahowald, N., Collins, W., Iacono, M.J., Bretherton, C.S., Flanner, M.G., and Mitchell, D.:
915 Toward a minimal representation of aerosols in climate models: description and evaluation in
916 the Community Atmosphere Model CAM5, *Geosci. Mod. Dev.*, 5, 709 – 739,
917 doi:10.5194/gmd-5-709-2012, 2012.

918 Loeb, N.G., Wielicki, B.A., Doelling, D.R., Smith, L., Keyes, D.F., Kato, S., Manalo-Smith, N.
919 and Wong, T.: Toward Optimal Closure of the earth’s top-of-atmosphere radiation budget, *J.*
920 *Climate*, 22, 748 – 766, 2009.

921 Ma, P.-L., Rasch, P.J., Fast, J.D., Easter, R.C., Gustafson Jr., W.I., Liu, X., Ghan, S.J. and Singh,
922 B.: Assessing the CAM5 physics suite in the WRF-Chem model: implementation, resolution
923 sensitivity, and a first evaluation for a regional case study, *Geosci. Model Dec.*, 7, 755 – 778,
924 2014.

925 Mass, C.: Improved subgrid drag or hyper PBL/vertical resolution? Dealing with the stable PBL
926 problems in WRF, presented at the 13th WRF Users’ Workshop, June 26 – 29, Boulder, CO,
927 2012.

928 Molders, N., Bruyere, C.L., Gende, S. and Pirhala, M.A.: Assessment of the 2006-2012
929 Climatological Fields and Mesoscale Features from Regional Downscaling of CESM Data by
930 WRF/Chem over Southeast Alaska, *Atmos. Clim. Sci.*, 4, 589 – 613, 2014.

931 Morrison, H., Thompson, G. and Tatarskii, V.: Impact of cloud microphysics on the development
932 of trailing stratiform precipitation in a simulated squall line: Comparison of One- and Two-
933 Moment Schemes, *Mon. Wea. Rev.*, 137, 991-1007, 2009.

934 Moss, R. H., Edmonds, J.A., Hibbard, K.A., Manning, M.R., Rose, S.K., van Vuuren, D.P.,
935 Carter, T.R., Emori, S., Kainuma, M., Kram, T., Meehl, G.A., Mitchell, J.F.B., Nakicenovic,
936 N., Riahi, K., Smith, S.J., Stouffer, R.J., Thomson, A.M., Weyant, J.P. and Wilbanks, T.J.:
937 The next generation of scenarios for climate change research and assessment, *Nature*, 463,
938 747 – 756, doi: 10.1038/nature0882, 2010.

939 Nasrollahi, N., AghaKouchak, A., Li, J., Gao, X., Hsu, K. and Sorooshian, S.: Assessing the
940 Impacts of Different WRF Precipitation Physics in Hurricane Simulations, *Wea. Forecasting*,
941 27, 1003 – 1016, 2012.

942 Neale R.B., Jadwiga, H.R., Conley, A.J., Park, S., Lauritzen, P.H., Gettelman, A., Williamson,
943 D.L., Rasch, P., Vavrus, S.J., Taylor, M.A., Collins, W.D., Zhang, M. and Lin, S.-J.:
944 Description of the NCAR Community Atmosphere Model (CAM 5.0), NCAR Tech. Note
945 NCAR/TN-486+STR, Natl. Cent. for. Atmos. Res., Boulder, CO, available at
946 http://www.cesm.ucar.edu/models/cesm1.0/cam/docs/description/cam5_desc.pdf, 2010, last
947 accessed July 6th, 2015.

948 Otte, T.L., Nolte, C.G., Otte, M.J. and Bowden, J.H.: Does Nudging squelch the extremes in
949 regional climate modeling? *J. Clim.*, 25, 7046 – 7066, doi:10.1175/JCLI-D-12-00048.1,
950 2012.

951 Penrod, A., Zhang, Y., Wang, K., Wu, S-Y. and Leung, R.L.: Impacts of future climate and
952 emission changes on U.S. air quality, *Atmos. Environ.*, 89, 533 – 547, 2014.

953 Petikainen, J.-P., O'Donnell, D., Teichmann, C., Karstens, U., Pfeifer, S., Kazil, J., Podzun, R.,
954 Fiedler, S., Kokkola, H., Birmili, W., O'Dowd, C., Baltensperger, U., Weingartner, E.,
955 Gehrig, R., Spindler, G., Kulmala, M., Feichter, J., Jacob, D. and Laaksonen, A.: The
956 regional aerosol-climate model REMO-HAM, *Geosci. Mod. Dev.*, 5, 1323 – 1339, 2012.

957 Pleim, J.E. and Gilliam, R.: An indirect data assimilation scheme for deep soil temperature in the
958 Pleim-Xiu Land Surface Model, *J. Appl. Meteor. Climatol.*, 48, 1362 – 1376, 2009.

959 Pouliot, G., van der Gon, H.A.C.D., Kuenen, J., Zhang, J., Moran, M. and Makar, P.: Analysis of
960 the Emission Inventories and Model-Ready Emission Datasets of Europe and North America
961 for Phase 2 of the AQMEII Project, *Atmos. Environ.*, in press,
962 doi:10.1016/j.atmosenv.2014.10.061, 2014.

963 Rawlins, M.A., Bradley, R.S. and Diaz, H.F.: Assessment of regional climate model simulation
964 estimates over the northeast United States, *J. Geophys. Res.*, 117, D23112,
965 doi:10.1029/2012JD018137, 2012.

966 Refslund, J., Dellwik, E., Hahmann, A.N., Barlage, M.J. and Boegh, E.: Development of satellite
967 green vegetation fraction time series for use in mesoscale modeling: application to the
968 European heat wave 2006, *Theor. Appl. Climatol.*, 117, 377-392, doi:10.1007/s00704-013-
969 1004-z, 2014.

970 Sarwar, G., Luecken, D.J. and Yarwood, G.: Developing and implementing an updated chlorine
971 chemistry into the Community Multiscale Air Quality Model, presented at the 28th
972 NATO/CCMS International Technical Meeting, Leipzig, Germany, May 15 – 19, 2006.

973 Sarwar, G., Luecken, D. and Yarwood, G.: Chapter 2.9: Developing and implementing an
974 updated chlorine chemistry into the community multiscale air quality model, *Developments*
975 *in Environmental Science*, Volume 6, C. Borrego and E. Renner (Eds.), Elsevier Ltd,
976 DOI:10.1016/S1474-8177(07)06029-9, 168 pp., 2007.

977 Sarwar, G., Fahey, K., Napelenok, S., Roselle, S. and Mathur, R.: Examining the impact of
978 CMAQ model updates on aerosol sulfate predictions, the 10th Annual CMAS Models-3
979 User's Conference, October, Chapel Hill, NC, 2011.

980 Shan, Z., Parol, F., Riedi, J., Cornet, C. and Thieuleux, F.: Examination of POLDER/PARASOL
981 and MODIS/Aqua cloud fractions and properties representativeness, *J. Climate*, 24, 4435 –
982 4450, 2011.

983 Sievering, H.: Small-particle dry deposition under high wind speed conditions: Eddy flux
984 measurements at the boulder atmospheric observatory, *Atmos. Environ.*, 21 (10), 2179 –
985 2185, 1987.

986 Tewari, M., Chen, F., Wang, W., Dudhia, J., LeMone, M.A., Mitchell, K., Ek, M., Gayno, G.,
987 Wegiel, J. and Cuenca, R.H.: Implementation and verification of the unified NOAA land
988 surface model in the WRF model. 20th conference on weather analysis and forecasting/16th
989 conference on numerical weather prediction, pp. 11 – 15, 2004.

990 Toth, T.D., Zhang, J., Campbell, J.R., Reid, J.S., Shi, Y., Johnson, R.S., Smirnov, A., Vaughan,
991 M.A. and Winker, D.M.: Investigating enhanced Aqua MODIS aerosol optical depth
992 retrievals over the mid-to-high latitude Southern Oceans through intercomparison with co-
993 located CALIOP, MAN and AERONET data sets, *J. Geophys. Res: Atmos*, 18, 1- 15, 2013.

994 van Vuuren, D.P., Edmonds, J., Kainuma, M., Riahi, K., Thomson, A., Hibbard, K., Hurtt, G.C.,
995 Kram, T., Krey, V., Lamarque, J.-F., Masui, T., Meinshausen, M., Nakicenovic, N., Smith,
996 S.J. and Rose, S.K.: The representative concentration pathways: an overview, *Climate*
997 *Change*, 109, 5 – 31, doi: 10.1007/s10584-011-0148-z, 2011.

998 Wang, K., Zhang, Y., Yahya, K., Wu, S.-Y. and Grell, G.: Implementation and initial
999 application of new chemistry-aerosol options in WRF/Chem for simulating secondary
1000 organic aerosols and aerosol indirect effects for regional air quality, *Atmos. Environ.*, in
1001 press, doi: 10.1016/j.atmosenv.2014.12.007, 2014a.

1002 Wang, K., Yahya, K., Zhang, Y., Hogrefe, C., Pouliot, G., Knote, C., Hodzic, A., San Jose, R.,
1003 Perez, J.L., Guerrero, P.J., Baro, R. and Makar, P.: Evaluation of Column Variable
1004 Predictions Using Satellite Data over the Continental United States: A Multi-Model
1005 Assessment for the 2006 and 2010 Simulations under the Air Quality Model Evaluation
1006 International Initiative (AQMEII) Phase 2, *Atmos. Environ.*, in press,
1007 doi:10.1016/j.atmosenv.2014.07.044, 2014b.

1008 Warrach-Sagi, K., Schwitalla, T., Wulfmeyer, V. and Bauer, H.-S.: Evaluation of a climate
1009 simulation in Europe based on the WRF-NOAH model system: precipitation in Germany,
1010 *Clim. Dyn.*, 41, 755 – 774, doi:10.1007/s00382-013-1727-7, 2013.

1011 Willmott, C. J.: On the validation of models, *Phys. Geog.*, 2, 184 – 194, 1981.

1012 Xing, J., Mathur, R., Pleim, J., Hogrefe, C., Gan, C.-M., Wong, D.C., Wei, C., Gilliam, R. and
1013 Pouliot, G.: Observations and modeling of air quality trends over 1990-2010 across the
1014 Northern Hemisphere: China, the United States and Europe, *Atmos. Chem. Phys.*, 15, 2723 –
1015 2747, doi:10.5194/acp-15-2723-2015.

1016 Xu, Z. and Yang, Z.-L.: An improved dynamical downscaling method with GCM Bias
1017 Corrections and Its Validation with 30 years of climate simulations, *J. Clim.*, 25, 6271 –
1018 6286, 2012.

1019 Yahya, K., Wang, K., Gudoshava, M., Glotfelty, T. and Zhang, Y.: Application of WRF/Chem
1020 over North America under the AQMEII Phase 2. Part I. Comprehensive Evaluation of 2006
1021 Simulation, *Atmospheric Environment*, in press, doi:10.1016/j.atmosenv.2014.08.063, 2014.

1022 Yahya, K., He, J., and Zhang, Y.: Multi-Year Applications of WRF/Chem over Continental U.S.:
1023 Model Evaluation, Variation Trend, and Impacts of Boundary Conditions over CONUS, *J.*
1024 *Geophy. Res.*, in review, 2015a.

1025 Yahya, K., Wang, K., Zhang, Y. and Kleindienst, T.E.: Application of WRF/Chem over North
1026 America under the AQMEII Phase 2. Part II. Comprehensive Evaluation of 2010 Simulation
1027 and Responses of Air Quality and Meteorology-Chemistry Interactions to Changes in
1028 Emissions and Meteorology from 2006 to 2010, *Geosci. Model Dev.*, in press, 2015b.

1029 Yarwood, G., Rao, S., Yocke, M. and Whitten, G.Z.: Final Report – Updates to the Carbon Bond
1030 Chemical Mechanism: CB05, Rep. RT-04-00675, 246 pp., Yocke and Co., Novato, Calif.,
1031 2005.

1032 Yu, S., Dennis, R., Roselle, S., Nenes, A., Walker, J., Eder, B., Schere, K., Swall, J., and
1033 Robarge, W.: An assessment of the ability of 3-D air quality models with current
1034 thermodynamic equilibrium models to predict aerosol NO₃-, *J. Geophys. Res.*, 110, D07S13,
1035 doi:10.1029/2004JD004718, 2005.

1036 Yu, S., Eder, B., Dennis, R., Chu, S.-H., and Schwartz, S.: New unbiased symmetric metrics for
1037 evaluation of air quality models, *Atmos. Sci. Lett.*, 7, 26 – 34, 2006.

1038 Yu, S., Mathur, R., Pleim, J., Wong, D., Gilliam, R., Alapaty, K., Zhao, C., and Liu, X.: Aerosol
1039 indirect effect on the grid-scale clouds in the two-way coupled WRF-CMAQ: model
1040 description, development, evaluation and regional analysis, *Atmos. Chem. Phys.*, 14, 11247 –
1041 11285, doi:10.5194/acp-14-1-2014, 2014.

1042 Zhang, Y., Liu, P., Pun, B., and Seigneur, C.: A comprehensive performance evaluation of
1043 MM5-CMAQ for summer 1999 Southern Oxidants Study Episode, Part-I. Evaluation
1044 Protocols, Databases and Meteorological Predictions, *Atmos. Environ.*, 40, 4825 – 4838,
1045 2006.

1046 Zhang, Y., Wen, X.-Y. and Jang, C.J.: Simulating chemistry-aerosol-cloud-radiation-climate
1047 feedbacks over the CONUS using the online-coupled Weather Research Forecasting Model
1048 with chemistry (WRF/Chem), *Atmos. Environ.*, 44, 3568 – 3582, 2010.

1049 Zhang, Y., Y.-C. Chen, G. Sarwar, and K. Schere, 2012a, Impact of Gas-Phase Mechanisms on
1050 Weather Research Forecasting Model with Chemistry (WRF/Chem) Predictions: Mechanism
1051 Implementation and Comparative Evaluation, *J. Geophys. Res.*, 117, D1,
1052 doi:10.1029/2011JD015775.

1053 Zhang, Y., P. Karamchandani, T. Glotfelty, D. G. Streets, G. Grell, A. Nenes, F.-Q. Yu, and R.
1054 Bennartz, 2012b, Development and Initial Application of the Global-Through-Urban
1055 Weather Research and Forecasting Model with Chemistry (GU-WRF/Chem), *J. Geophys.*
1056 *Res.*, 117, D20206, doi:10.1029/2012JD017966.

1057

1058

Table 1. Model configurations and set-up

Model Attribute	Configuration	Reference
Domain and Resolutions	36km × 36km, 148 × 112 horizontal resolution over continental U.S., with 34 layers vertically from surface to 100 hPa	-
Simulation Period	January 2001 to December 2010	-
Chemical and Meteorological ICs/BCs	Downscaled from the modified Community Earth System Model/Community Atmosphere Model (CESM/CAM5) v1.2.2; Meteorological ICs/BCs bias-corrected with National Center for Environmental Protection's Final (FNL) Operational Global Analysis data	He et al. (2014) Glotfelty et al. (2015)
Biogenic Emissions	Model of Emissions of Gases and Aerosols from Nature (MEGAN2)	Guenther et al. (2006)
Dust Emissions	Atmospheric and Environmental Research Inc. and Air Force Weather Agency (AER/AFWA)	Jones and Creighton (2011)
Sea-Salt Emissions	Gong et al. parameterization	Gong et al. (1997)
Radiation	Rapid and accurate Radiative Transfer Model for GCM (RRTMG) SW and LW	Clough et al. (2005) Iacono et al. (2008)
Boundary Layer	Yonsei University (YSU)	Hong et al. (2006) Hong (2010)
Land Surface	National Center for Environmental Prediction, Oregon State University, Air Force and Hydrologic Research Lab (NOAH)	Chen and Dudhia (2001) Ek et al. (2003) Tewari et al. (2004)
Microphysics	Morrison double moment scheme	Morrison et al. (2009)
Cumulus Parameterization	Grell 3D Ensemble	Grell and Freitas (2014)
Gas-phase chemistry	Modified CB05 with updated chlorine chemistry	Yarwood et al. (2005) Sarwar et al. (2006) Sarwar et al. (2007)
Photolysis	Fast Troposphere Ultraviolet Visible (FTUV)	Tie et al. (2003)
Aqueous-phase chemistry	AQ chemistry module (AQCHEM) for both resolved and convective clouds	Based on AQCHEM in CMAQv4.7 of (Sarwar et al. 2011)
Aerosol module	MADE/VBS	Ahmadov et al. (2012)
Aerosol Activation	Abdul-Razzak and Ghan	Abdul-Razzak and Ghan (2000)

Table 2. The 10-year (2001 – 2010) average performance statistics for the simulated meteorological, aerosol, cloud, radiation variables, and chemical species against surface observational networks and satellite retrieval products.

Database and Variable	Mean Obs	Mean Sim	R	MB	NMB (%)	NME (%)
NCDC T2 (°C)	12.5	12.2	1.0	-0.3	-2.6	7.9
NCDC RH2 (%)	68.4	70.8	0.8	2.4	3.5	6.8
NCDC WS10 (m s ⁻¹)	3.54	3.84	0.3	0.3	8.6	28.4
NCDC WD10 (deg)	151.4	180.0	0.2	28.6	18.9	22.0
NADP Precip (mm day ⁻¹)	18.0	26.3	0.5	8.3	45.9	65.1
CERES SWDOWN (W m ⁻²)	184.1	184.6	0.8	0.5	0.3	8.4
CERES GSW (W m ⁻²)	157.5	151.8	0.8	-5.7	-3.6	9.6
CERES GLW (W m ⁻²)	323.3	325.7	1.0	2.4	0.7	1.8
CERES OLR (W m ⁻²)	240.0	224.8	0.6	-15.0	-6.3	6.3
MODIS AOD	0.14	0.10	0.1	-0.03	-24.0	38.5
MODIS CLDFRA	58.3	62.0	0.7	3.7	6.4	11.9
MODIS-derived CDNC (cm ⁻³)	169.8	130.0	0.4	-39.9	-23.5	38.0
MODIS CWP (g m ⁻²)	179.5	170.0	0.3	-9.6	-5.3	61.2
MODIS COT	16.5	9.2	0.2	-7.3	-44.3	54.0
CERES SWCF (W m ⁻²)	-41.8	-49.6	0.5	7.8	18.6	31.4
CERES LWCF (W m ⁻²)	24.8	31.8	0.6	6.9	28.0	34.7
AQS Hourly O ₃ (ppb)	29.3	32.1	0.6	2.8	9.7	22.4
AQS Max 1-hr O ₃ (ppb)	48.9	49.7	0.6	0.8	1.7	7.9
AQS Max 8-hr O ₃ (ppb)	43.7	45.9	0.6	2.2	5.0	9.3
CASTNET Hourly O ₃ (ppb)	35.0	31.9	0.7	-3.1	-8.8	19.8
CASTNET Max-1hr O ₃ (ppb)	47.4	38.5	0.4	-8.9	-18.8	31.4
CASTNET Max 8-hr O ₃ (ppb)	43.3	37.9	0.5	-5.4	-12.5	29.6
AQS 24-hr PM ₁₀ (µg m ⁻³)	22.5	11.0	0.1	-11.5	-51.2	57.1
IMPROVE PM _{2.5} (µg m ⁻³)	5.33	6.57	0.4	1.2	23.3	53.4
STN PM _{2.5} (µg m ⁻³)	12.0	10.7	0.2	-1.3	-10.8	38.3
IMPROVE SO ₄ ²⁻ (µg m ⁻³)	1.45	1.86	0.8	0.4	28.0	41.8
STN SO ₄ ²⁻ (µg m ⁻³)	3.10	3.74	0.7	0.6	20.7	36.8
IMPROVE ¹ NO ₃ ⁻ (µg m ⁻³)	0.54	0.44	0.7	-0.1	-17.9	64.6
STN NO ₃ ⁻ (µg m ⁻³)	1.62	0.70	0.4	-0.9	-56.9	65.3
IMPROVE NH ₄ ⁺ (µg m ⁻³)	1.02	0.72	0.4	-0.3	-29.6	45.5
STN NH ₄ ⁺ (µg m ⁻³)	1.34	1.05	0.5	-0.3	-21.5	38.7
IMPROVE EC (µg m ⁻³)	0.23	0.16	0.6	-0.1	-30.7	48.3
STN EC (µg m ⁻³)	0.65	0.38	0.2	-0.3	-42.0	52.8
IMPROVE OC (µg m ⁻³)	1.10	1.88	0.2	0.8	71.7	134.6
IMPROVE TC (µg m ⁻³)	1.33	2.05	0.2	0.7	53.9	116.3
STN TC (µg m ⁻³)	4.42	2.42	0.1	-2.0	-45.3	69.7

¹ NH₄⁺ IMPROVE data only available up to 2005.

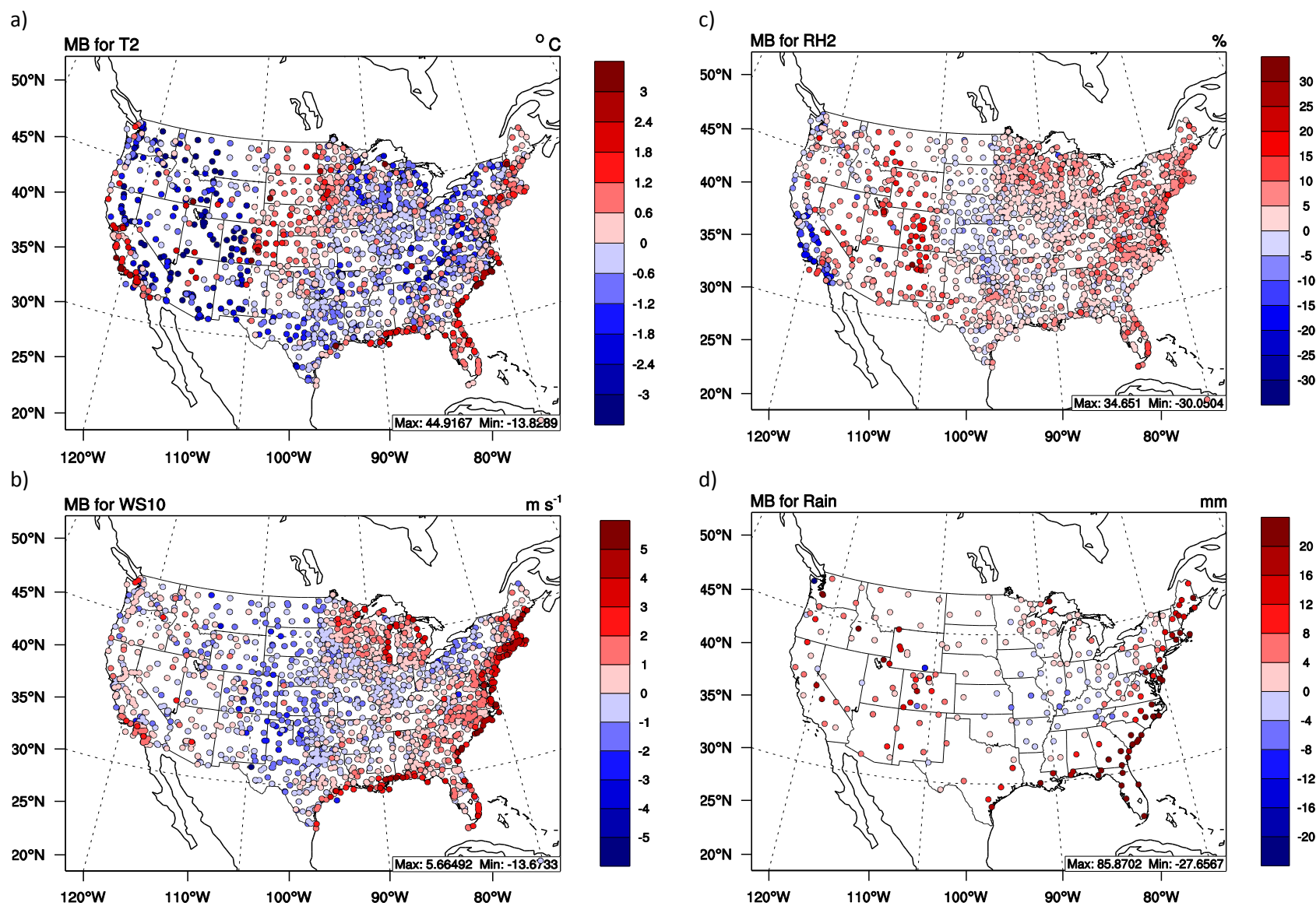


Figure 1. Spatial distribution of MBs for: a) 2-m temperature (T2), b) 2-m relative humidity (RH2), c) 10-m wind speed (WS10) from NCDC, and d) weekly precipitation from NADP. Each marker represents the MB of each variable at each observational site.

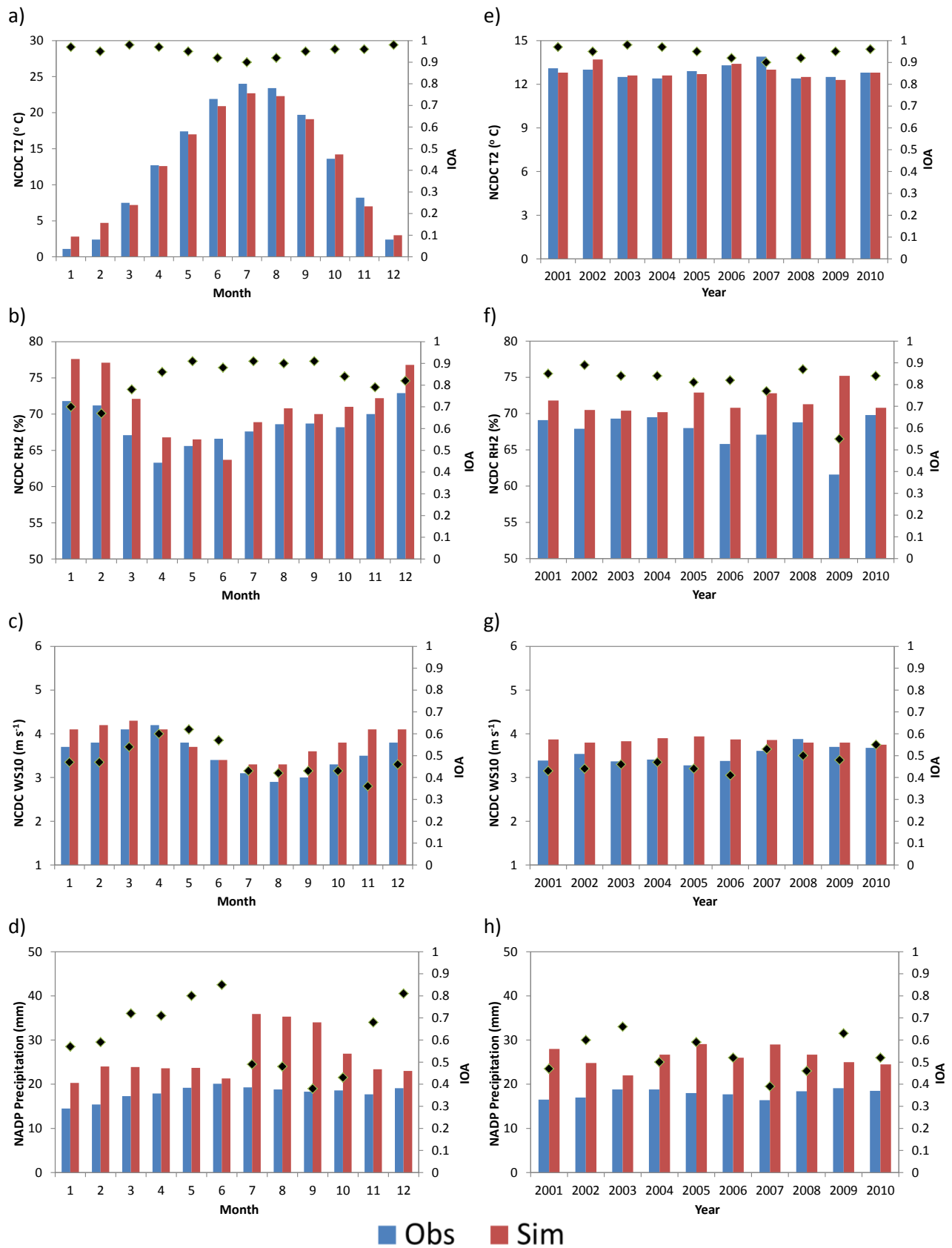


Figure 2. Time series of 10-year averaged monthly observations (blue) versus simulations (red) for: a) T2, b) RH2, and c) WS10 against NCDC data, and d) precipitation against NADP data, and annual averages for e) T2, f) RH2, and g) WS10 against NCDC data, and h) precipitation against NADP. IOA statistics (black diamonds) are also provided on the secondary y-axes in panels a) – h).

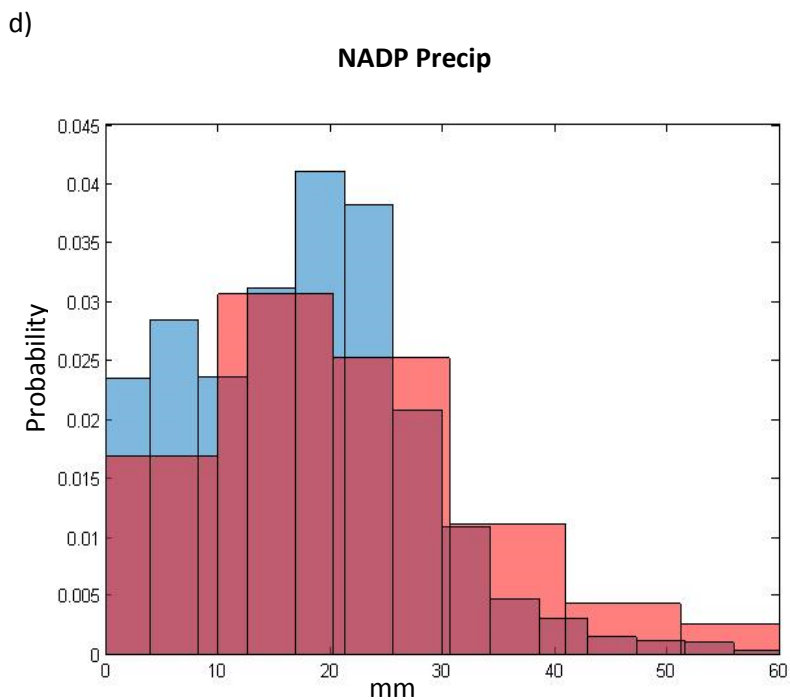
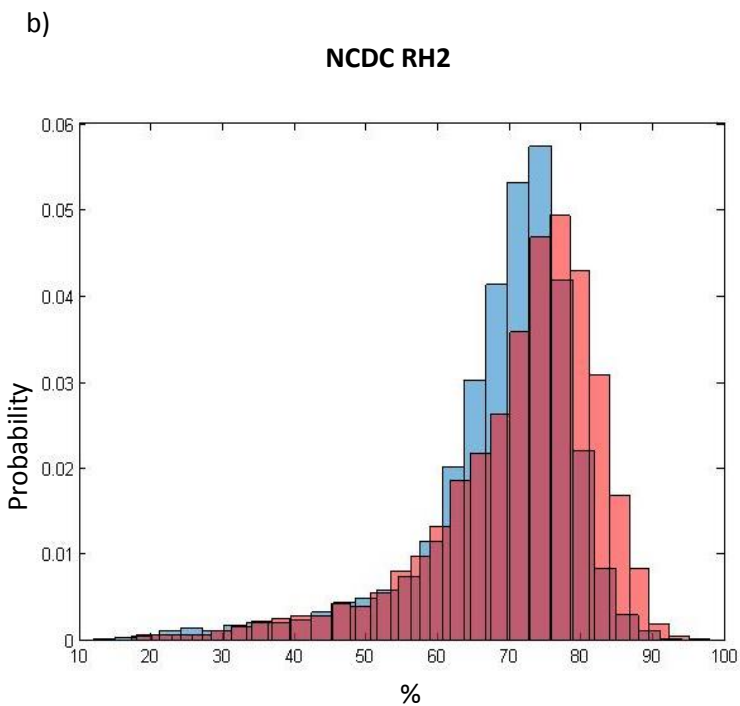
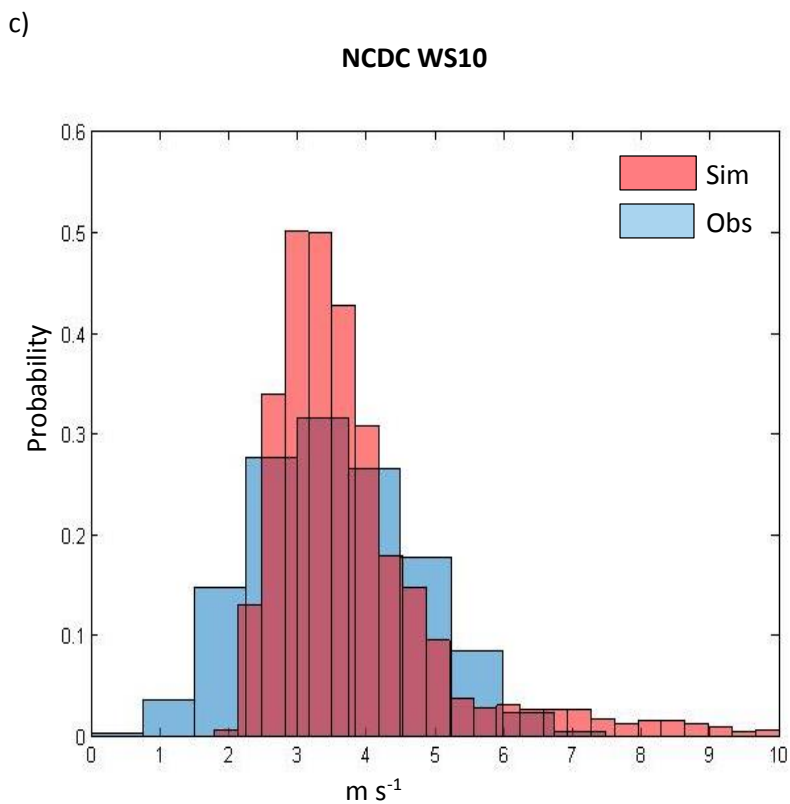
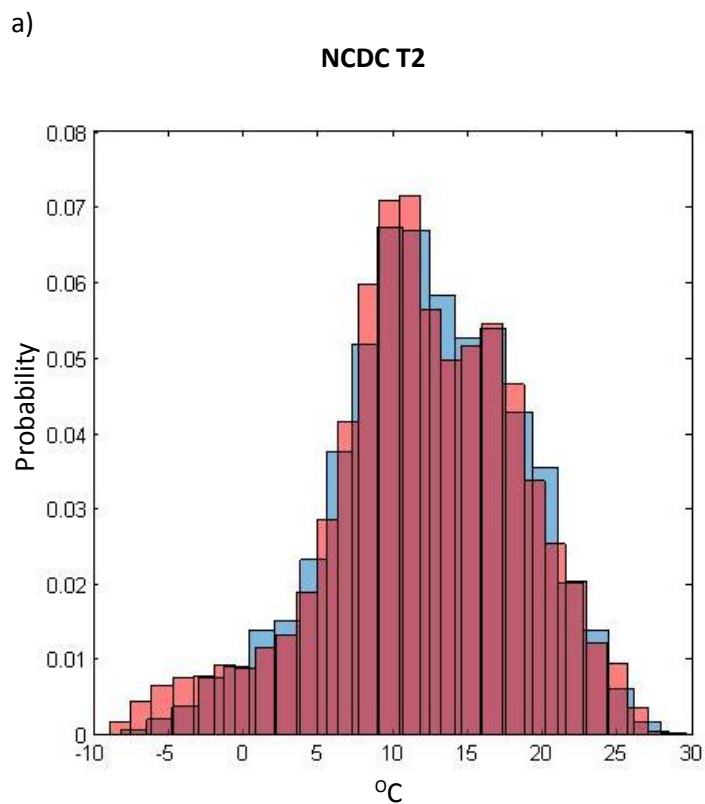


Figure 3. Probability distribution functions (PDFs) of a) T2, b) RH2, c) WS10 against NCDC, and d) precipitation against NADP for 2001 to 2010 over 30 bins in the respective ranges for all variables.

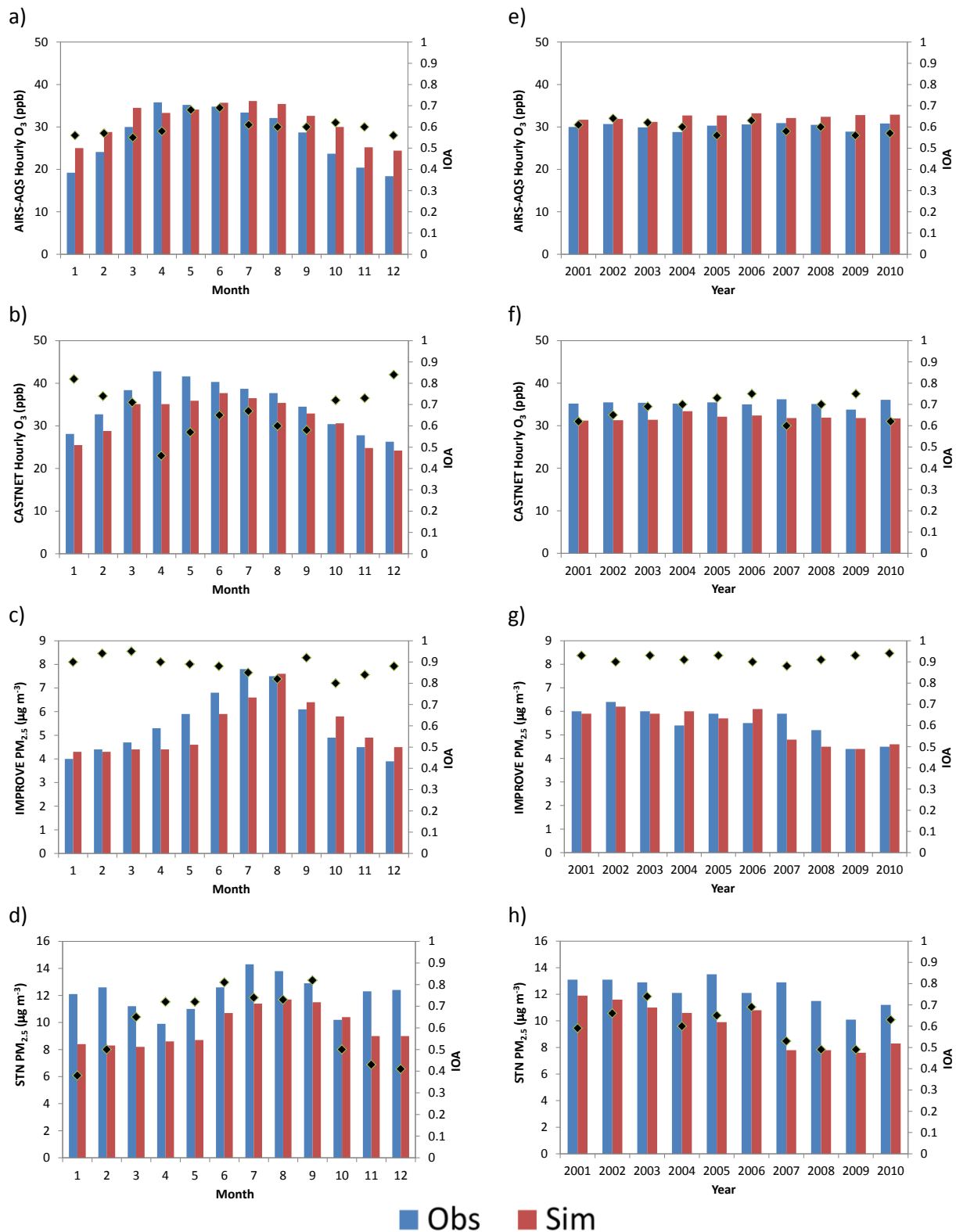


Figure 4. Time series of 10-year averaged monthly-mean observations (blue) versus simulations (red) for: a) O₃ against AQS data, b) O₃ against CASTNET data, c) PM_{2.5} against IMPROVE, and d) PM_{2.5} against STN, and annual averages for e) O₃ against AQS data, f) O₃ against CASTNET data, g) PM_{2.5} against IMPROVE, and h) PM_{2.5} against STN. IOA statistics (black diamonds) are also provided on the secondary y-axes in panels a) – h).

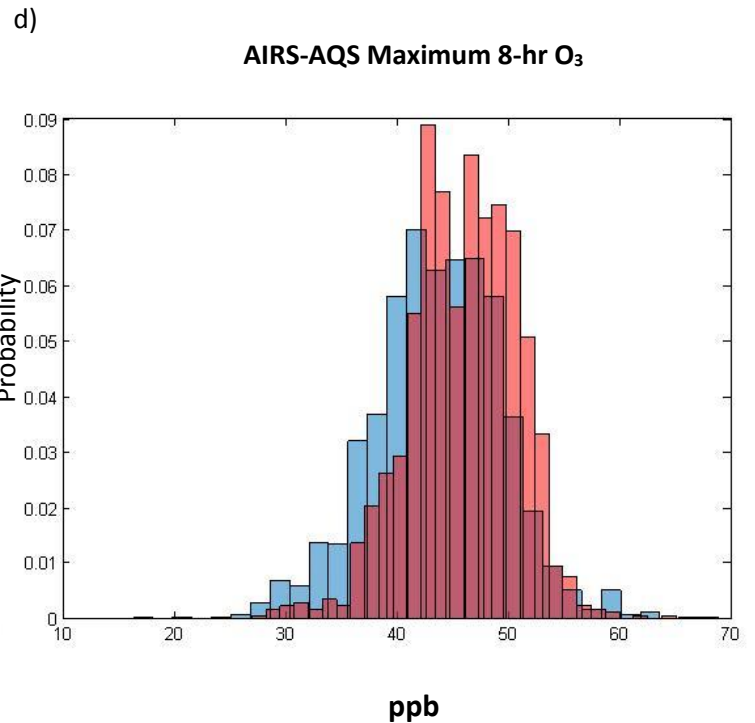
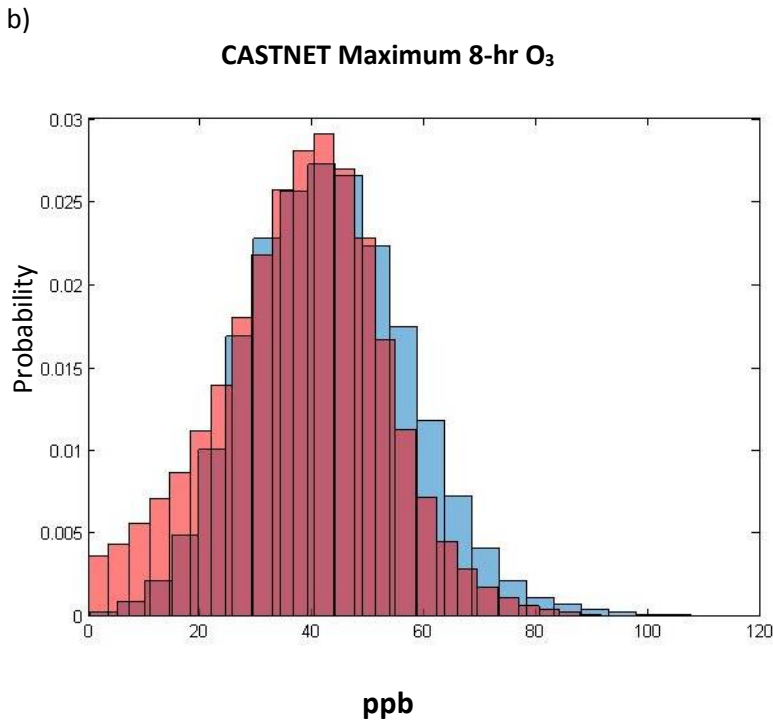
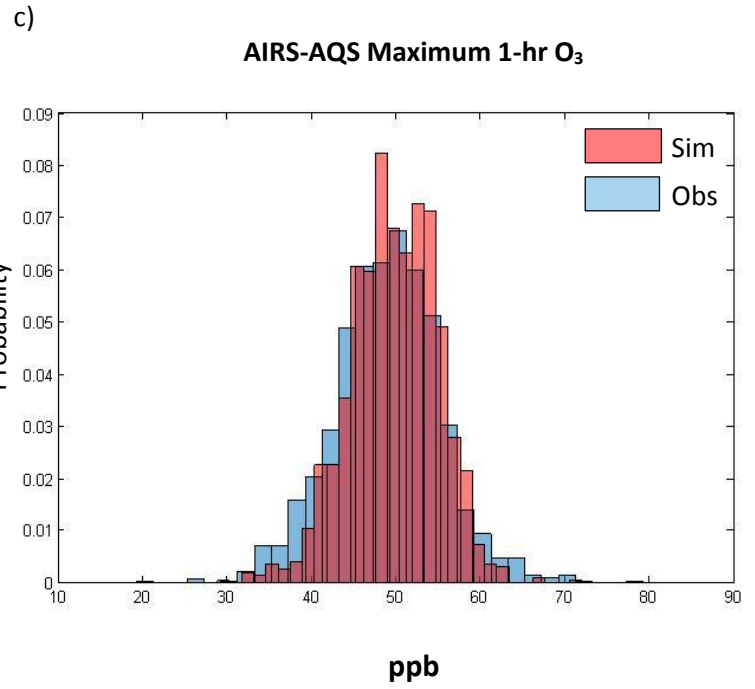
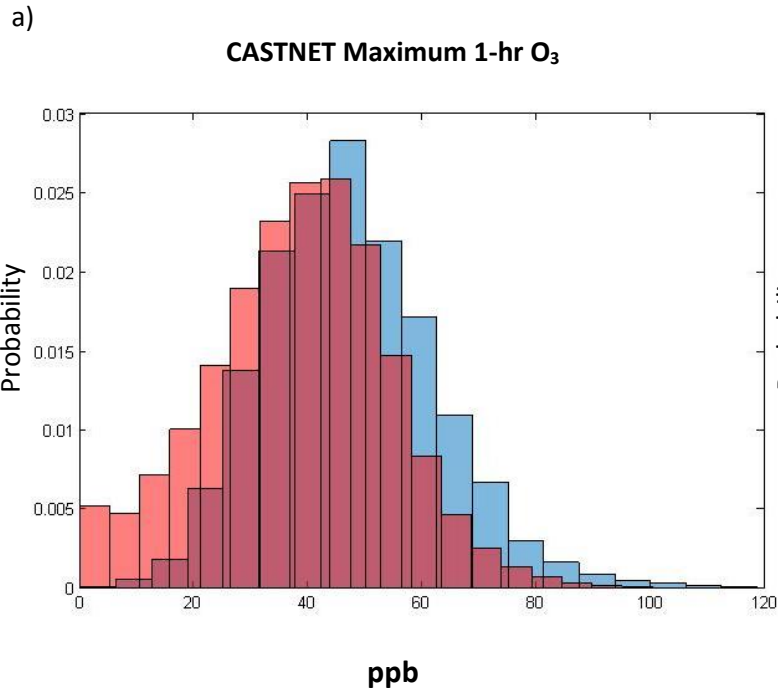


Figure 5. Probability distribution functions (PDFs) of a) maximum 1-hr O₃ against CASTNET, b) maximum 8-hr O₃ against CASTNET, c) maximum 1-hr O₃ against AIRS-AQS, and d) maximum 8-hr O₃ against AIRS-AQS for 2001 to 2010 over 30 bins in the respective ranges for all variables.

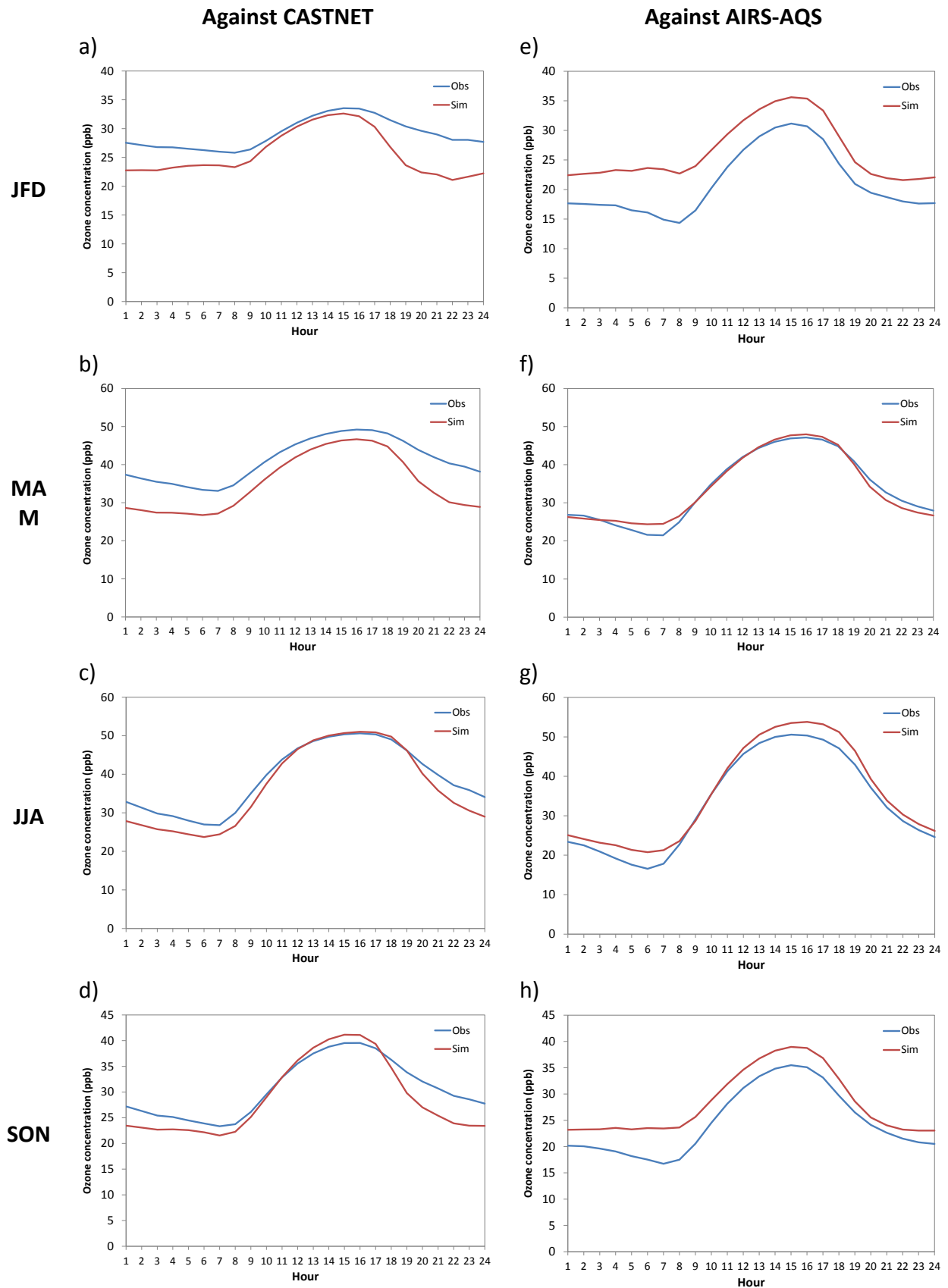


Figure 6. Diurnal variation of observed vs. simulated hourly O_3 concentrations against CASTNET (left column from a) to d)) and AIRS-AQS (right column from e) to h)) for all climatological seasons. The x-axes refer to hours in local standard time.

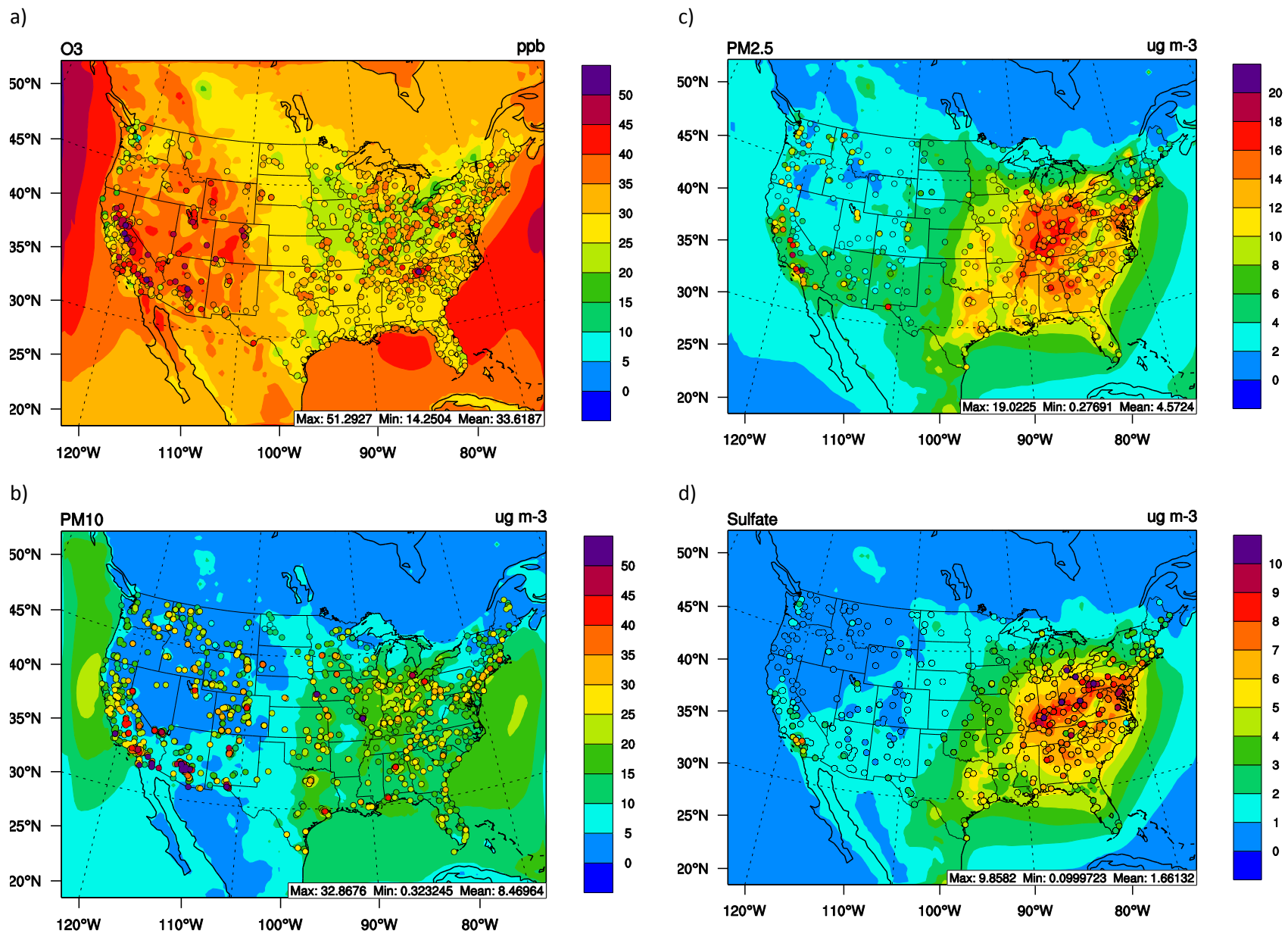


Figure 7. Spatial distribution of 10-year averaged hourly observed vs. simulated a) O₃ for CASTNET and AIRS-AQS, b) PM₁₀ from AIRS-AQS, c) PM_{2.5}, and d) PM_{2.5} sulfate from STN and IMPROVE. The background plots represent the simulated data while observations are represented by the markers.

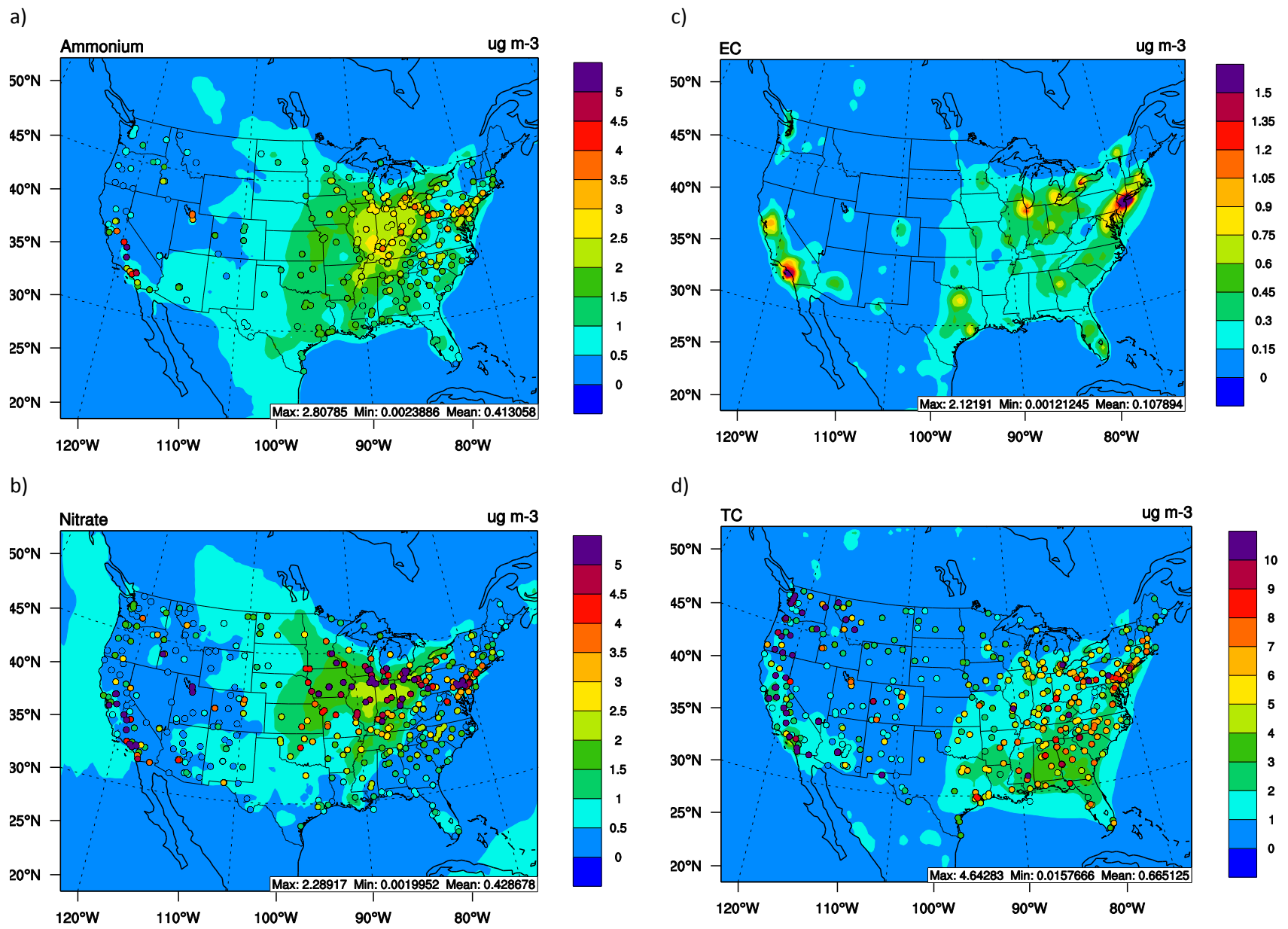


Figure 8. Spatial distribution of 10-year averaged hourly observed vs. simulated a) Ammonium, b) Nitrate, c) EC, and d) TC from STN and IMPROVE. The background plots represent the simulated data while observations are represented by the markers.

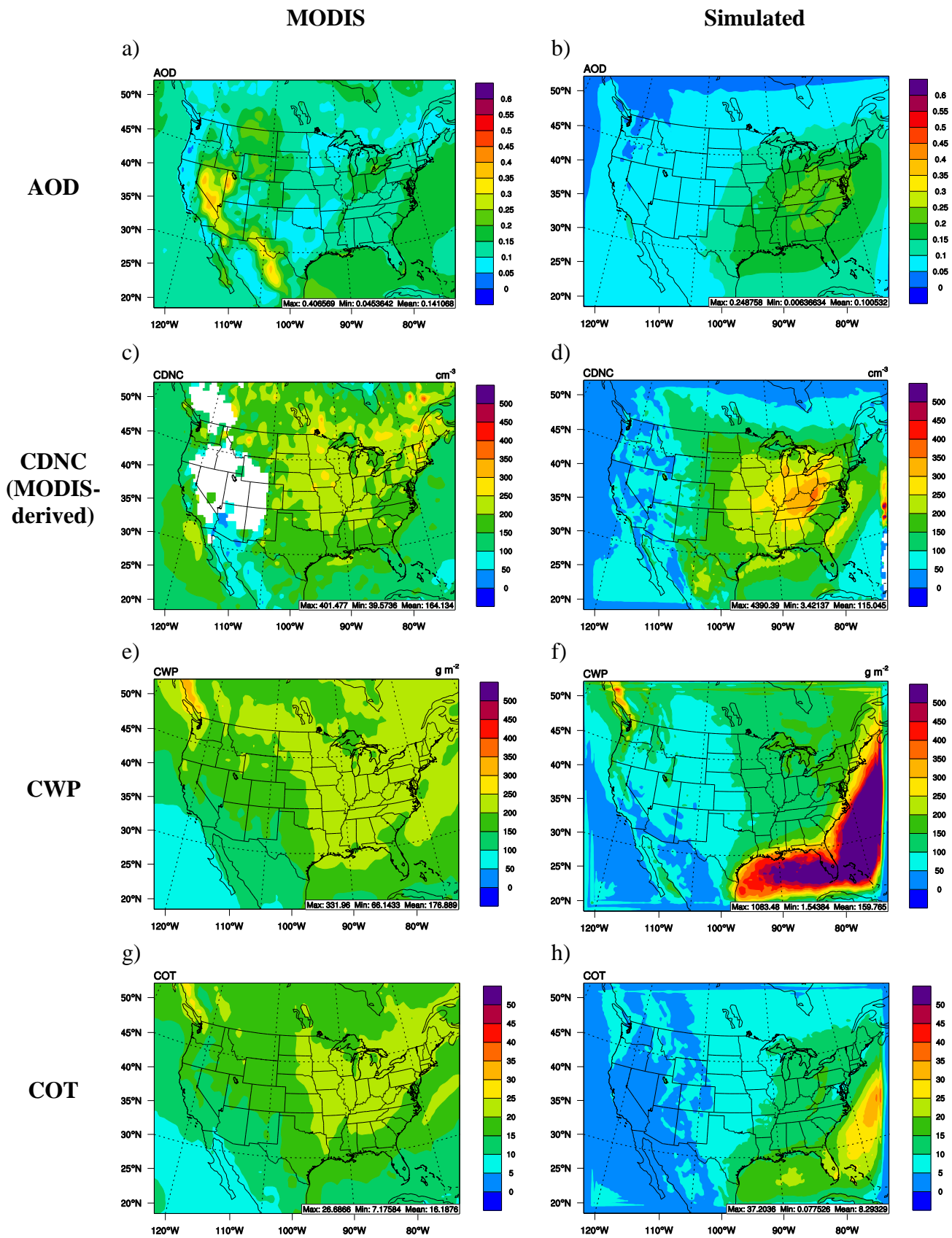


Figure 9. 10-year averaged MODIS (left) vs. simulated (right) AOD (a and b), CDNC (c and d), CWP (e and f), and COT (f and g).

